Ingineria automobilului

Registrul Auto Român
SIAR
Societatea Inginerilor de Automobile din România

SE DISTRIBUIE GRATUIT CA SUPLIMENT AL REVISTEI AUTOTEST
Nr. 43 / iunie 2017

KART LOW COST

Model pentru anticiparea performanțelor și emisiilor poluante ale unui motor diesel alimentat cu motorină și biodiesel B20. Simulare și validare ● Constrângeri geometrice pentru un mecanism de distribuție cu contact sferic între culbutor și capul supapei ● Analiza distrucțiilor acoperirilor caroseriei autovehiculelor la contactul cu excrementele păsărilor marine în zona litorală a Mării Negre ● Studiu prin simulare numerică privind consumul de combustibil al unui vehicul hibrid și emisiile eliberate în ambient ● Modelarea proceselor termodinamice în compresoarele cu unde de presiune

SIAR ESTE MEMBRĂ FISITA INTERNATIONAL FEDERATION OF AUTOMOTIVE ENGINEERING SOCIETIES
EAEC EUROPEAN AUTOMOBILE ENGINEERS COOPERATION

CONAT 2016 – The 12th International Congress

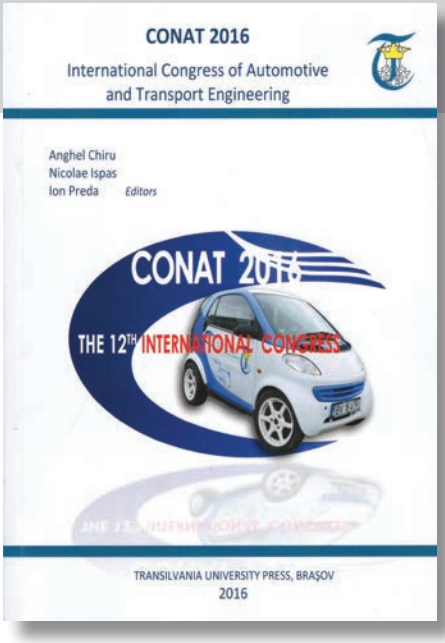

Editori: **Anghel CHIRU, Nicolae ISPAS, Ion PREDA**

Editura: Transilvania University Press, Brașov
Anul apariției: 2016
ISSN 2069-0401 (Print)
ISSN 2069-0428 (CD)

Lucrarea cuprinde o serie de lucrări prezentate în cadrul Congresului Internațional de Inginerie a Autovehiculelor și Tranporturilor - CONAT 2016, organizat în perioada 26 – 29 Octombrie 2016 de către Societatea Inginerilor de Automobile din România și Universitatea Transilvania din Brașov.
Volumul este constituit din trei secțiuni astfel:
- Main Section – cuprinde un număr de 22 articole prezentate în secțiunile tehnice ale congresului;
- Student Section – prezintă un număr de 9 articole întocmite de studenți;
- Poster Section – include 12 postere cu realizări studențești.
Lucrarea, împreună cu cele două volume editate de Springer, constituie „Proceedings of the International Congress of Automotive and Transport Engineering – CONAT 2016".

MODELAREA ȘI SIMULAREA SISTEMELOR DE PROPULSIE PENTRU AUTOMOBILE

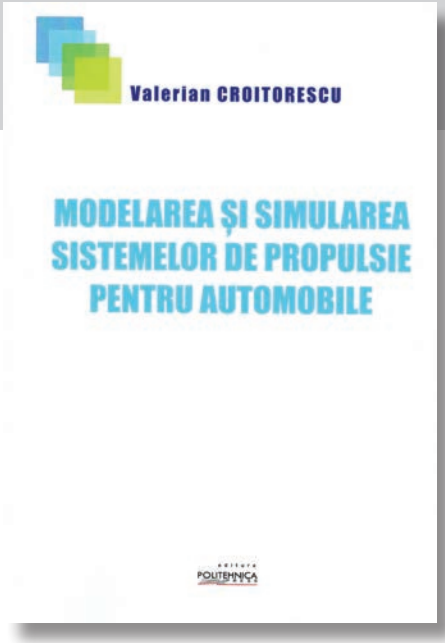

Autor: **Valerian CROITORESCU**

Editura: Politehnica Press, București
Anul apariției: 2016
ISBN 978-606- 515-695-1

Lucrarea prezintă modalități actuale de modelare, simulare și validare a sistemelor de pe automobil, cu precădere a sistemului de propulsie și a elementelor componente ale acestuia. Ea descrie modalitățile prin care se justifică necesitatea utilizării modelării și simulării unui sistem de pe automobil, pornind de la principiile de bază ale dezvoltării sistemelor și modelelor funcționale asociate acestora. De asemenea, evidențiază principiile și cerințele dezvoltării standurilor de testare în buclă în timp real și componența acestora. Validarea unui prototip virtual constă în dezvoltarea unui sistem de testare în buclă în timp real, în care, suplimentar modelului de simulare, se va regăsi fizic cel puțin un element component al sistemului modelat. Lucrarea prezintă un exemplu de configurație a standurilor ce pot fi folosite pentru testarea în buclă în timp real a unei transmisii cu variație continuă și a unei mașini electrice reversibile cu reluctanță variabilă utilizate într-un sistem de propulsie hibrid electric.
Lucrarea este structurată pe cinci capitole și mai cuprinde o introducere și lista bibliografică:
Introducere
1. Stadiul actual al soluţiilor de interes
2. Arhitectură funcţională. Mărimi caracteristice. Organizare generală
3. Criterii de selecţie
4. Dezvoltare modele geometrice
5. Dezvoltare modele funcţionale
Bibliografie

DESPRE SIGURANȚA CIRCULAȚIEI: SECURITATE PASIVĂ, UN ECE, NCAP, FIMCAR...

ABOUT ROAD SAFETY: PASSIVE SAFETY, UN ECE, NCAP, FIMCAR...

Siguranța circulației definește o noțiune complexa și conține componente care adaugă un număr ridicat de variabile și incertitudini acestui sistem. Elementele componente sunt de natura diferită și se referă la om – conducător auto; pieton; biciclist sau altfel de participant la trafic, autovehicul, viteza de deplasare, cale rutieră și trafic rutier. Buna desfășurare a traficului și efectuarea unei călătorii fără incidente este condiționată de capacitatea de adaptare a omului la condițiile și cerințele traficului rutier. Adaptarea presupune și utilizarea adecvată a mijlocului de transport fără producerea unor evenimente de natură să perturbe buna desfășurare a traficului.

Având în vedere faptul că un obiectiv urmărit în proiectarea autovehiculelor și a căilor rutiere este creșterea vitezei de deplasare devine necesară utilizarea unor soluții tehnice constructive de natură să reducă riscul de apariție a unui eveniment rutier sau a minimiza consecințele în cazul în care un eveniment rutier se produce. În acest sens sunt definite categoriile de metode și mijloace tehnice utilizate pentru a preveni – securitatea activă și pentru a proteja – securitatea pasivă.

In condiții normale de trafic controlul vitezei de deplasare se realizează prin intermediul sistemelor autovehiculului ce pot fi asistate de sisteme electronice suplimentare care au rolul de a îmbunătăți performanțele de mers.

În cazul în care se produce un eveniment rutier prin devierea de la traiectoria normală de deplasare și producerea unei coliziuni, energia cinetică a autovehiculului va trebui să fie consumată prin deformarea controlată a elementelor structurii de rezistență a autovehiculului. Această deformare trebuie să fie controlată și nu trebuie să permită deformări ale habitaclului sau expunerea ocupanților autovehiculul la accelerații crescute. Riscul de rănire și gravitatea traumei este sporită atât în cazul contactului cu structuri ale autovehiculului cât și urmare a variației într-un interval de timp foarte scurt (de ordinul milisecundelor) a vitezei autovehiculului.

Asigurarea acestei performanțe se realizează prin încercări complexe care necesită echipamente tehnice specializate (instalații de coliziune). Modalitatea de încercare precum și cerințele sunt indicate de normele specifice UN ECE (United Nations Economic Commission for Europe) și, în general, sunt de tipul trece / nu trece.

Din dorința de a completa informațiile disponibile referitoare la nivelul de siguranță oferit de autovehicule a fost constituită o organizație independentă al cărei scop este de a informa publicul în mod obiectiv. Cercetările independente se desfășoară sub denumirea NCAP (New Car Assessment Programme). Procedurile de încercare derivă din normele UN ECE însă sporesc cu 30% energia cinetică a autovehiculului de încercat aducând în acest sens un plus de dificultate în definirea soluțiilor tehnice de protecție prin creșterea capacității de utilizare.

Pentru evaluarea rezultatelor se folosește un sistem de punctare bazat pe acordarea de stele. Comportamentul autovehiculului în timpul impactului prin asigurarea unui nivel ridicat de protecție este evaluat corespunzător prin acordarea a maxim cinci stele.

Interesant este faptul că începând cu anul 2016 NCAP utilizează un sistem dual de evaluare și efectuează teste pentru autovehiculul cu echipare standard cât și pentru cel care are adăugate măsuri de siguranță disponibile ca opțiuni la cumpărare. Rezultatele pot fi interpretate ca avantaj al utilizării tuturor soluțiilor tehnice disponibile (suplimentar) sau, plecând de la punctajul maxim obținut, ca implementări tehnice necesare pentru a spori siguranță autovehiculului standard prin evaluarea/re-evaluarea structurii de rezistență.

Cu toate că sunt dificil de implementat, soluțiile care oferă un nivel ridicat de siguranță sunt cele care utilizează metode avansate de proiectare a structurii autovehiculului și utilizarea unor materiale cu performanțe structurale îmbunătățite. Desigur că această metodă este mai costisitoare, însă în viitor va pune din ce în ce mai mult la încercare inginerii proiectanți, avându-se în vedere faptul că pentru siguranță activă sunt necesare echipamente suplimentare care cresc masa autovehiculul în detrimentul performanțelor de consum și a emisiilor poluante.

Atât normele UN ECE cât și protocolul NCAP fac referire doar la autovehiculul de încercat și se referă la performanța oferită în cazul încercării la impact cu o structură de referință (barieră).

În prezent se constată o varietate a dimensiunilor autovehiculelor capabile de a se deplasa cu viteze ridicate, ceea ce adaugă cerințe specifice legate de compatibilitatea structurilor de rezistență. O inițiativă a fost lansată prin programul FIMCAR (Frontal Impact and Compatibility Assessment Research) și are ca potențială soluție de implementare unei viitoare norme UN ECE. Va fi interesant de urmărit acest demers pentru că adoptarea și apoi implementarea unei astfel de măsuri va conduce la dezvoltarea unor noi soluții tehnice.

Până atunci o soluție de rezolvare a securității pasive cu toate elementele bune sau mai puțin bune este reprezentată de om – conducător auto – și utilizarea rațională a mijlocului de transport disponibil.

Ștefan TABACU, Prof. univ. dr. habil. ing.
Departamentul Autovehicule și Transporturi
Universitatea din Pitești

SUMAR „INGINERIA AUTOMOBILULUI" NR. 43

Coperta 1: Imagini surprinse la competiția Kart Low Cost 2017, Nevers, Franța

REGISTRUL AUTO ROMÂN

Director general
George-Adrian DINCĂ
Director tehnic
Cristian Viorel BUCUR
Director economic
Mihaela GHEORGHE
Director dezvoltare
Gabriel Florentin TUDORACHE

Șef Birou Comunicare și Redacție Revistă Auto Test
Roxana NICA

Redactori
Radu BUHĂNIȚĂ
Emilia PETRE
George DRUGESCU
Gabriel MANOLE

Contact:
Calea Griviței 391 A,
sector 1, cod poștal 010719,
București, România
Tel/Fax: 021/202.70.17
E-mail: autotest@rarom.ro
www.rarom.ro
www.autotestmagazin.ro

SIAR

Contact
Facultatea de Transporturi
Universitatea Politehnica București
Splaiul Independenței 313
Sala JC 005, Cod poștal 060042,
sector 6, București, România
Tel/Fax: 021/316.96.08
E-mail: siar@siar.ro
www.ingineria-automobilului.ro
www.siar.ro

TIPAR
S.C. TIPOGRAFIA PRODCOM S.R.L.
Str. Lt. Col. Dumitru Petrescu nr. 20
Târgu-Jiu

Ingineria automobilului: an apariție ediția tipărită 2006 (ISSN 1842 – 4074) / ediția electronică 2007 (ISSN 2284 – 5690).
Serie nouă a Revistei Inginerilor de Automobile (RIA), tipărită în perioada 1990-2000 (ISSN 1222-5142)
SIAR publică online Romanian Journal of Automotive Engineering ISSN 2457 – 5275

MODEL FOR PREDICTING THE PERFORMANCE AND EXHAUST GAS EMISSIONS OF A DIESEL ENGINE FUELLED BY DIESEL AND BIODIESEL B20. SIMULATION AND VALIDATION

MODEL PENTRU ANTICIPAREA PERFORMAȚELOR ŞI EMISIILOR POLUANTE ALE UNUI MOTOR DIESEL ALIMENTAT CU MOTORINĂ ŞI BIODIESEL B20. SIMULARE ŞI VALIDARE

REZUMAT

Creșterea cererii, a prețului și epuizarea resurselor de combustibili fosili au impus în întreaga lume cercetări pentru identificarea unor surse alternative de energie pentru motoarele cu ardere internă. Dintre numeroasele varinate, biodieselul este considerat ca un combustibil promițător pentru motoarele Diesel.

Această lucrare este orientată pe studiul motoarelor alimentate cu motorină și biodiesel B20. Se propune un model care să furnizeze informații credibile privind performațele motorului, carateristicile combustiei, emisiile de gaze pentru diverse turații ale motorului în plină sarcină. Se prezintă rezultatele simulărilor obținute prin folosirea AVL BOOST v2013.2. Aceste rezultate sunt validate pe baza datelor experimentale

Key-words: *Biodiesel, diesel engine, performance, emissions.*

Drd. ing. **Mohanad ALDHAIDHAWI**[1,2]
mohanadhamazah@gmail.com

Prof. dr. ing. **Viorel BĂDESCU**[2]

Prof. dr. ing. **Radu CHIRIAC**[1]

[1] Al-Furat Al-Awsat Technical University, Technical Intitute of Kufa, Iraq
[2] Universitatea Politehnica din București, Splaiul Independenței, Nr. 313, București, România

Table 1. Engine specifications used in the test

Tractor Diesel engine	4 stroke, vertical cylinder Diesel
No. of cylinder	4 in line
Bore x stroke (mm)	102 x 115
Displacement (cm^3)	3759
Combustion system	Direct injection (DI)
Maximum torque (Nm) @1400rpm	228
Max Rated output(kW) @2400rpm	50
Compression ratio	17.6

1. INTRODUCTION

Presently, there has been a global increase in investigations concerning the application of alternative fuels for daily use, such as Biodiesel and its blends as a fuel in Diesel engine. This universal search for alternative fuel is connected to the fact that the world population continues to grow and the limited amount of petroleum fuels begin to diminish, it may not be possible to provide the amount of energy demanded by the world by only using petroleum fuels to convert energy. Moreover, there is an awareness of the global concern regarding air pollution caused by the extensive use of petroleum fuels in internal combustion engines. Biodiesel was found to possess similar physical properties to those of Diesel fuel, and can be used in Diesel engines either directly or mixed with Diesel fuel, without any change of the original adjustments of the engine were prepared by the manufacture [1]. Biodiesel has some advantages which make it an acceptable fuel substitute to Diesel fuel in the future, such as renewable energy, lower sulfur and aromatics contents, safe to handle and store, better lubrication, improved biodegradability and decreased toxicity [2][3]. In addition, Biodiesel has a higher cetane number compared to Diesel fuel, whose influence results in a shorter ignition delay time and then improved fuel combustion [4]. On the other hand, the higher viscosity of Biodiesel can be twice that of Diesel depending on the feedstock, and production significantly suppresses Biodiesel's fuel flow, fuel spray evaporation, and atomization process, which led to an increase in the combustion duration and resulted in slower burning [5][6]. During the last decade, many researchers attempted to produce accurate models to predict engine performance and exhaust emissions with different types of software. Perhaps one of the most useful aspects of engine modeling is that the simulation allows the user to imagine different scenarios, being able to see on a computer screen the temporal variations of pressure, volume and gas flow rate that take place during the engine cycle. Today, Diesel engines occupy a prominent role in current power generation, transportation sector and in most passenger cars due to the fact that the Diesel engine is considered more efficient and durable than the gasoline engine. Many methods have been tried and are in use to reduce pollutant emissions from Diesel engines. The one solution to reduce pollutants is the use Biodiesel and adopting some modifications to the combustion process [7][8]. Numerical simulations of the Diesel engine can be used to understand its combustion characteristics, formulated exhaust gas emissions, and engine performance behavior, and these simulations can reduce the costs and effort.

Racovitza et al. [9] have investigated, by numerical and experimental study, the performance and emission characteristics of Biodiesel B20 at different starts of fuel injection (-7 degree (standard) and down to -44 degree) at 2400 rpm engine speed and 60% engine loads. These results indicated that the engine performance and efficiency of the tested engine maintain their reference values (SOI -7) a slight increase of BSFC when B20 is used; they explained that this behavior is due to a lower heating value and higher density of Biodiesel B20 compared to that of Diesel fuel.

Harch et al [10] developed an engine combustion model (which

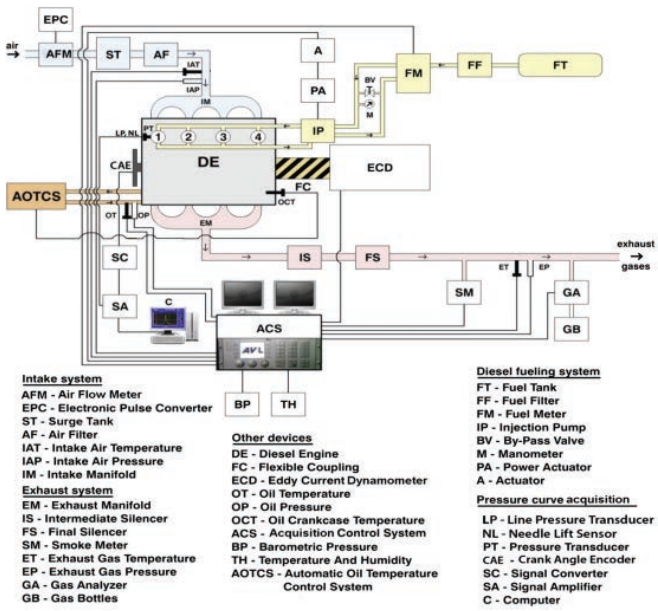

Fig. 1. Schematic diagram of the engine setup

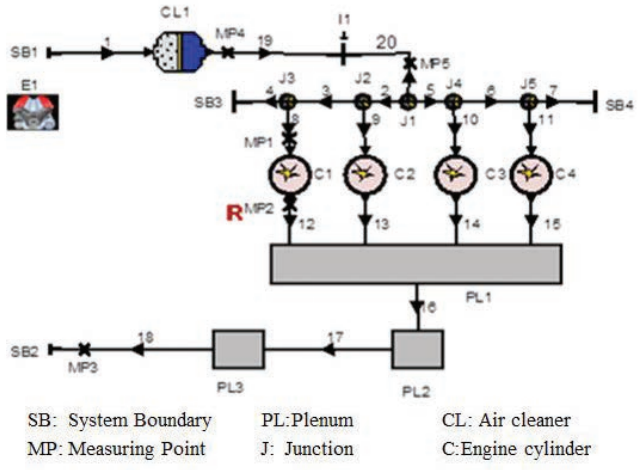

Fig. 2. Schematic of the engine symbolic model (AVL BOOST Theory and AVL BOOST Users Guide)

involves fuel atomization, burning velocity, combustion duration, temperature, and pressure) for a Diesel engine fuelled with second generation Biodiesel blends (B5 and B10) by using computational fluid dynamics (CFD) software and AVL Fire. The simulation results revealed that B10 provides better performance and efficiency, and significantly reduced engine emissions, while the B5 blend provides slightly improved performance and efficiency, and moderately reduced emissions compared to petroleum Diesel. The purpose of this study is to present a model of a tested direct injection Diesel engine in order to simulate engine performance and exhaust gas emissions by using simulation tools called AVL Boost. The outcome of this modeling work is validated against experimental data.

2. EXPERIMENTAL INFRASTRUCTURE

A four-cylinder, four-stroke, naturally-aspirated, water-cooled, direct injection tractor Diesel engine coupled to an eddy-current dynamometer equipped with a load controller was used in this study. The basic engine specifications are shown in Table 1. The fuel injector has five 0.24 mm diameter holes with an opening pressure of 330 bars. Two AVL GM 12 D pressure transducers with sensitivity 15.76pC/bar were used to measure the in cylinder pressure and one AVL QL21D pressure transducer with sensitivity 2.5pC/bar and maximum measuring range of 3000 bar was used to measure high pressure line values. For the purpose of analyzing the regulated gasses produce by the diesel engine, a Horiba Mexa 7170 D Gas Analyzer was used. Figure 1 illustrates the schematic diagram for the engine instrumentation [11]. The test bed operating using multiple fuels has been adapted for the purpose of the present work, allowing the engine to be alternatively fueled with tested fuels, i.e. Diesel and Biodiesel B20. The engine was initially fuelled with Diesel fuel until it achieved engine operation stability. All tests were done with Diesel fuel in order to provide the baseline data and then the fuel was switched to Biodiesel B20. Before stopping the test engine after each test with Biodiesel fuel, the engine was switched back to Diesel fuel operation until all the Biodiesel based blend was purged from the fuel lines, injection pump, and injector, to avoid clogging. The performance and emissions of the engine were monitored and registered at engine speed (1400 rpm, 2000 rpm and 2400 rpm), full load, and the injection

Table 2. Calibration parameter values for diesel and biodiesel B20

Parameter	Diesel (D), Biodiesel (B20) at full load					
	1400 rpm		2000 rpm		2400 rpm	
	D	B20	D	B20	D	B20
Number of injector holes (-)	5					
Hole diameter (mm)	0.24					
Discharge coefficient (DisC) (-)	0.7					
Rail pressure (RaiP) (bar)	350					
Injection delay calibration factor (IgnDel) (-)	0.45	0.30	0.72	0.30	0.72	0.43
Combustion parameter (ComPar) (-)	1.3	1.18	1.32	1.25	1.38	1.50
Turbulence parameter (TurPar) (-)	1					
Dissipation parameter (DisPar) (-)	1.2	1.2	1	1	1	0.8
Premixed combustion parameter (PremixPar) (-)	0.5	0.18	0.21	1.2	0.23	1.2
NoX kinetic multiplier (NO KM) (-)	1.79	1.7	1.62	1.57	1.62	1.6
NOx post processing multiplier (NO PM)(-)	0.21	0.19	0.165	0.16	0.160	0.30
CO kinetic multiplier (COKM)(-)	0.026	0.016	0.029	0.018	0.03	0.02
EGR parameter (EGRPar)(-)	1					
Evaporation Parameter (EvaPar)(-)	0.70353					

Table 3. Comparison between simulation and experimental results at (1400, 2000, 2400 rpm) and full load for Diesel and Biodiesel B20

Fuel	T_e[N.m]		P_e[kW]		BSFC[g/kWh]		BTE[%]		NOx[ppm]		CO[ppm]	
1400 rpm												
	Num	Exp	Num	Exp	Num	Exp	Num	Exp	Num	Exp	Num	Exp
Diesel	221.5	224.2	32.5	32.87	239.29	236.38	35.99	36.43	1048.49	944	839.4	866
St. dev	1.208%		1.125%		-1.269%		1.208%		3.097%		-3.070%	
B20	218.1	216.4	32.17	31.73	250.96	254.96	33.8	33.3	1060	1017	642	639
St. dev	-0.785%		-1.386%		1.568%		-1.519%		-4.228%		-0.469%	
2000 rpm												
	Num	Exp	Num	Exp	Num	Exp	Num	Exp	Num	Exp	Num	Exp
Diesel	202.8	204.7	42.5	42.88	249.53	247.2	34.52	34.84	697.78	739	363	446
St. dev	0.493%		0.886%		-0.942%		0.918%		5.57%		-4.310%	
B20	204.7	203.9	42.86	42.7	252.95	253.80	34.46	34.34	755	789	358	388
St. dev	-0.392%		-0.375		0.337%		-0.332%		4.309%		7.732%	
2400 rpm												
	Num	Exp	Num	Exp	Num	Exp	Num	Exp	Num	Exp	Num	Exp
Diesel	190. 38	188.5	47.9	47. 37	252.45	255.014	34.11	33.77	624.91	640	470	612
St. dev	-0.997%		-1.119%		1.005%		-1.007%		2.357%		-3.070	
B20	188.9	186.3	47.47	46.83	257.89	261.798	34.619	34.188	713	727	550	539
St. dev	-1.395		-1.367%		1.493%		-1.261%		1.926%		-2.041%	

timing was experimentally determined for all engine operating conditions based on the injector needle lift curve. In-cylinder pressure data were averaged over 200 consecutive engine cycles. The large number of cycles was to cancel out the random noise. The performance and emissions results were acquired from the average of three stable and continuously measured values.

3. SIMULATION PROCEDURES

In the present work, the simulation model was created using the AVL BOOST simulation program in order to develop an analysis regarding engine operation and performances under the AVL- MCC combustion model and the Woschni 1990 heat transfer model. The chemical and physical properties of Diesel fuel are provided by the AVL Boost program, whereas for Biodiesel B20 they have been implemented to the program by the authors of this paper. This represents one of the main contributions of the added by the authors of the paper. The engine calibration parameters and cylinder processes' simulation were described by using code v2013.2 (AVL BOOST Theory and AVL BOOST Users Guide). Hence, the engine components, such as the intake and exhaust manifolds, the cylinders geometry, the air filter, the system boundaries, the catalyst were implemented in the Boost interface based on the real values which were taken from the engine used in this study, that have been modeled in [11]. All the components were chosen are linked together by pipes as shown Figure 2.

The Start and the rate of fuel injection, mass flow rate of air and fuel were experimentally measured and implemented in the AVL BOOST program for every specified engine speed and test fuels at full load. A group of parameters related to performance, combustion and emissions was changed in this visual manner, in order to fit the output experimental data with the simulation results. Hence, many runs of the program were repeated for the accurate determination of the combustion model's parameters .The calibration parameter values were chosen considering the AVL- MCC combustion model and the Woschni 1990 heat transfer model for which the operating data on injection and combustion characteristics would provide acceptable relative errors. These parameter values are listed in table 2 for Diesel and Biodiesel B20 fuels at full load and variety speeds.

Computer output (effective power, effective torque, BSFC, cylinder

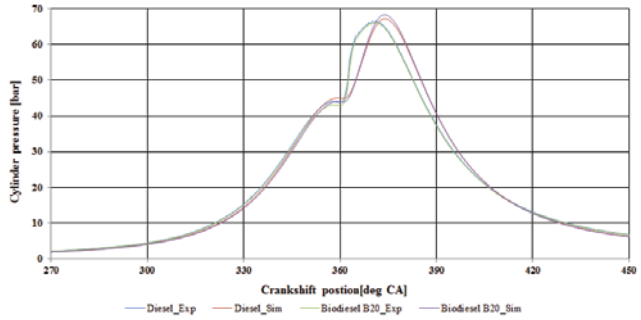

Fig. 3. Comparison between experimental and simulation pressure traces for full load, 1400 rpm speed

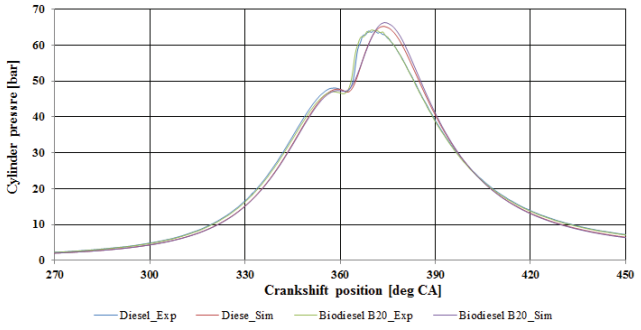

Fig. 4. Comparison between experimental and simulation pressure traces for full load, 2000 rpm speed

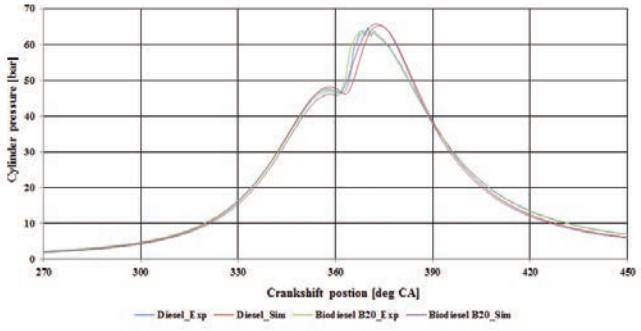

Fig. 5. Comparison between experimental and simulation pressure traces for full load, 2400 rpm speed

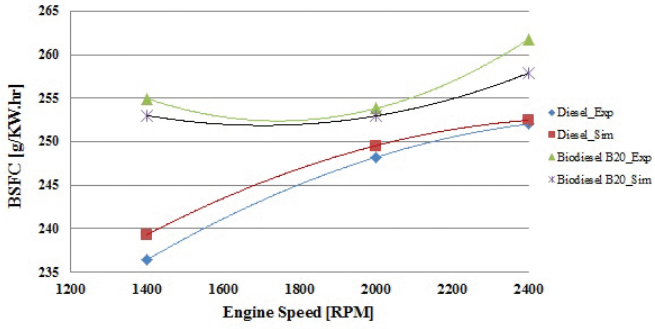

Fig. 6. Brake specific fuel consumption vs. engine speed at full load

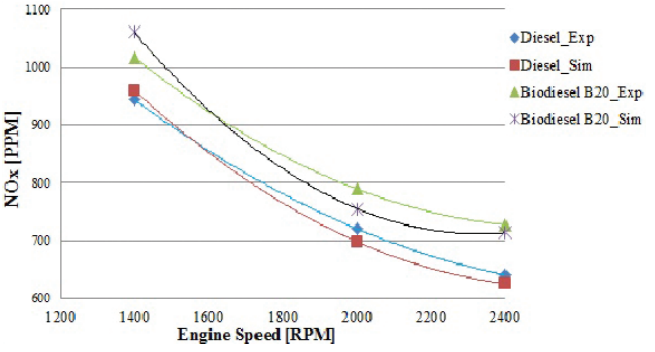

Fig. 7. Nitrogen Oxides (NOx) vs. engine speed at full load

pressure, cylinder temperature, NOx, CO, cylinder temperature, the rate of heat release…. etc.) is traditionally provided in the form of numbers, and analysis graphs are normally created after the computation process. The outcome of this modeling work was validated against the experimental data as discussed in Section 2.

4. RESULTS AND DISCUSSION

A simulation model was built in AVL Boost to investigate the effect of Biodiesel B20 fuel on engine performance and exhaust gas emission. The results were divided in two groups: first group compares the numerical results with the experimental results to test the usefulness of the model. The second group presents the effect of Biodiesel B20 on the brake specific fuel consumption, Nitrogen oxide (NOx), cylinder temperature and rate of heat release. All data were taken at different engine speeds (1400 rpm, 2000 rpm, and 2400rpm), at full applied loads and fuel supplies of pure Diesel and B20.

4.1. Cylinder pressure

The variations of cylinder pressure in respect to the crank angle, experimental and simulation for Diesel and Biodiesel B20 at varied engine speeds and full load operation are given in Figures (3- 5). Good agreement between the pressure traces, experimental and simulation, for all engines speeds and test fuels , has been observed. The relative variation between the experimental and numerical in maximum cylinder pressure for Diesel fuel at engine speeds of 1400 rpm, 2000 rpm and 2400 rpm were 0.61 %, 1.75% and 1.108 % respectively, whereas for Biodiesel B20 they were 2.51 %, 3.1%, and 2.61%, respectively.

4.2. Engine performance

The engine performance, efficiency indicators and exhaust gas emissions at engine speeds (1400 rpm, 2000 rpm, and 2400 rpm) with full load for Diesel and B20 fuels, simulation results with relative variations concerning the experimental result are presented in Table 3. The oxygen content 10-12% of Biodiesel B20 with higher cetane number contributed in improved the combustion process resulting in a reduction in CO emission .Moreover, Biodiesel B20 has higher density and lower heating value than Diesel fuel resulting in increased fuel consumption to produce the same output power. The brake thermal efficiency (BTE) was decreased with B20 compared to Diesel fuel. Overall operation conditions; Biodiesel B20 produced lower effective power (P_e) and effective torque (T_e). Hence, it is concluded that the simulation model carried out using the AVL Boost program has a wide scope for any microanalysis of combustion characteristics, engine performance and exhaust gas emissions. The results of the present models are in good agreement with the experimental results.

4.3. Brake Specific Fuel Consumption (BSFC)

The variation of brake specific fuel consumption (BSFC) with respect to engine speeds, at full load when fueled with pure Diesel and B20, predicted by the experimental and simulation model is given in Figure 6. From this figure, it can be observed that the BSFC is lower at low engine speeds and increases slightly by increasing the engine speed for the both tested fuel. The BSFC was higher with Biodiesel B20 than Diesel fuel overall operation conditions. The explanation of this increase in BSFC is due to the fact that Biodiesel has lower calorific value and higher density than Diesel fuel resulting in increased fuel consumption to produce the same engine output. This increasing in BSFC for Biodiesel is in agreement with existing literature [1][12]. The simulation results related to BSFC are in accordance with the experimental dada and similar curve trends can be observed.

4.4. Nitrogen Oxides (NOx)

The production of NOx emissions is influenced by the in-cylinder temperature, availability of oxygen (O_2) and residence time. Figure 7 presents the variation of nitrogen oxides (NOx) with respect to engine speeds when fuelled with Diesel and Biodiesel B20 at full load. Overall operation conditions, the Biodiesel B20 produced higher NOx emissions compared to Diesel fuel. The NOx emissions increased by 1.12%, 7.578% and 12.354% at engine speeds of 1400 rpm, 2000 rpm , and 2400 rpm respectively, over Diesel fuel. This may be due to decreased radiation heat transfer due to lower soot concentration and highest oxygen content of Biodiesel can be associated with higher post flame temperature, explaining higher NOx emission. Relative to the experimental, the simulation results were in good agreement and similar curve trends can be observed.

4.5. Cylinder Temperature

The variation of cylinder temperature respect to the crank angle at engine speed 2400 rpm, 2000 rpm and 1400 rpm under full load operation for Diesel and B20 shown in figure 8. Biodiesel B20 produced higher temperature overall operation conditions compared to Diesel fuel. The higher cetane number of the B20 fuel and present the oxygen during the combustion resulting in a complete combustion, this may be the main explanations for the increase in the cylinder temperature.

4.6. Rate heat release

Figure 9 compares the apparent rates of heat release for Diesel and Biodiesel B20 at the engine speed of 2400 rpm, 2000 rpm and 1400 rpm at full engine load predicted by the simulation model. At lower engine speed the rate of heat release pattern is similar for Diesel and Biodiesel B20, while at higher engine speed Biodiesel B20 has lower rate of heat

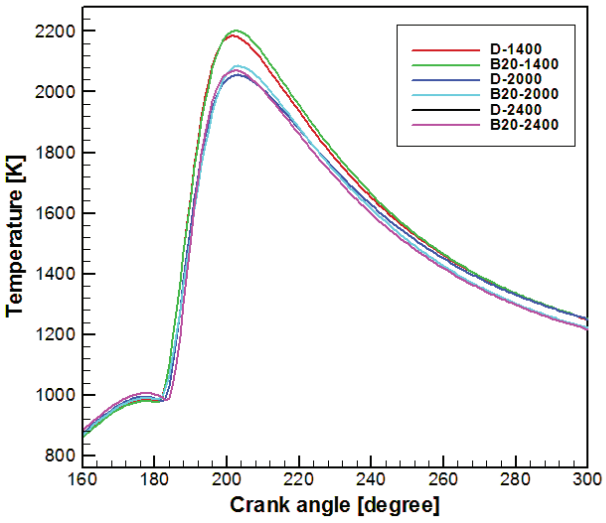

Fig. 8. Temperature as a function of crank angle during combustion

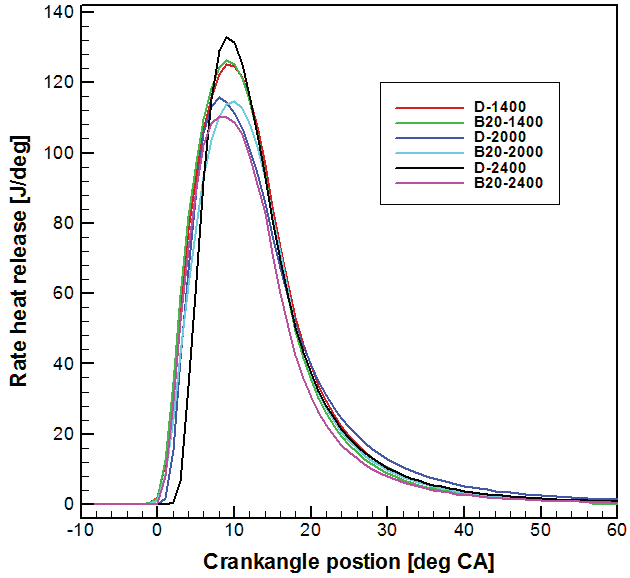

Fig. 9. Rate Heat release as a function of crank angle during combustion

release during the mixing controlled combustion. This is probably due to the fact that Biodiesel B20 has lower volatility and higher viscosity. However, figure 9 reveals that the Biodiesel B20 produces lower rate of heat release for all engine speeds and this may be attributed to the fact that Biodiesel B20 has lower heating value compared to Diesel fuel.

5. CONCLUSION

A comprehensive simulation model created using AVL Boost was developed to predict the combustion characteristics, engine performance, and exhaust gas emission. The simulation results were validated against experimental results. Four cylinders, four strokes, naturally- aspirated and direct injection Diesel engine was used in this study. The results were collected at different engine speeds (1400 rpm, 2000 rpm, and 2400 rpm and full load conditions fueled with pure Diesel and Biodiesel B20. This model predicted the engine performance characteristics and exhaust gas emissions, and it was found that the model has been successful in correctly predicting the trend for effective torque, effective power, brake thermal efficiency, BSFC, and NOx emissions. The rate of heat release is found lower for B20 due to lower heating value .The BSFC was found to be higher for B20 at all engine speeds when compared to that of Diesel fuel , due to the fact that Biodiesel has a lower heating value and higher density than that of Diesel. A slight increase in NOx emissions was observed when using Biodiesel B20 fuel.

ACKNOWLEDGEMENT

The authors of this paper acknowledge the AVL Advanced Simulation Technologies team for the significant support they have offered in performing the simulation part of this work. One of author (Mohanad ALDHAIDHAWI) thanks the Iraqi government for financial support.

Lucrare prezentată în cadrul Congresului Internațional de Inginerie a Autovehiculelor și Transporturilor - CONAT 2016, 26.10 – 28.10.2016, Brașov, România, și publicată în Proceedings of the Congress (ISSN 2069-0401).

REFERENCES:

[1] Ozturk, E.: *Performance, emissions, combustion and injection characteristics of a Diesel engine fuelled with canola oil–hazelnut soap stock Biodiesel mixture*. Fuel Processing Technology. 129, 183-191 (2015)

[2] Shahabuddin, M., Kalam, M., Masjuki, H., Bhuiya, M., Mofijur, M.: *An experimental investigation into Biodiesel stability by means of oxidation and property determination*. Energy.44,616–22 (2012)

[3] Sadeghinezhad, E., Kazi, S.N, Sadeghinejad, F., Badarudin, A., Mehrali, M., Rad Sadri, R. , Safaei, M.R.: *A comprehensive literature review of bio-fuel performance in internal combustion engine and relevant costs involvement* . Renewable and Sustainable Energy Reviews. 30, 29-44 (2014)

[4] Sharon, H., Ram, PJ.S., Fernando, K.J, Murali, S. , Muthusamy, R.:*Fueling a stationary direct injection Diesel engine with Diesel-used palm oil–butanol blends – An experimental study.* Energy Conversion and Management. 73,95–105 (2013)

[5] Celikten, I. , Koca , A. , Arslan, M. : *Comparison of performance and emissions of Diesel fuel, rapeseed and soybean oil methyl esters injected at different pressures*. Renewable Energy. 35,814–820 (2010)

[6] Beatrice C, Napolitano P and Guido C . : *Injection parameter optimization by DoE of a light-duty Diesel engine fed by Bio-ethanol/RME/Diesel blend*. Applied Energy.113, 373–384 (2014)

[7] Buyukkaya, E.: *Effects of Biodiesel on a DI Diesel engine performance, emission and combustion characteristics*. Fuel. 89 ,3099–3105 (2010)

[8] Lesnik, L., Iljaz, J., Hribernik, A., Kegl, B.: *Numerical and experimental study of combustion, performance and emission characteristics of a heavy-duty DI Diesel engine running on Diesel, Biodiesel and their blends*. Energy Conversion and Management .81, 534–546 (2014)

[9] Racovitza, A., Radu, B., Aldhaidhawi, M. Chiriac, R.: *On The Possibility to Reduce Diesel Engines Emissions by Operating with Biodiesel B20 in PPC Mode*. Proceedings of the European Automotive Congress EAEC-ESFA: 405-418(2015)

[10] Harch, C. A., Rasul, M. G., Hassan, N. M. S., Bhuiya, M. M. K.: *Modelling of Engine Performance Fuelled with Second Generation Biodiesel*. Procedia Engineering.90,459 – 465 (2014)

[11 Chiriac, R., Racovitza, A., Podevin, P., Descombes, G. : *On the Possibility to Reduce CO2 Emissions of Heat Engines Fueled Partially with Hydrogen Produced by Waste Heat Recovery*, International Journal of Hydrogen Energy. 40, 15856-15863 (2015)

[12] Bari ,S.: *Performance, combustion and emission tests of a metro-bus running on Biodiesel ULSD blended (B20) fuel*. Applied Energy. 124, 35–43 (2014).

NUMERICAL SIMULATION STUDY OF A HYBRID ROAD VEHICLE REGARDING FUEL ECONOMY AND AMBIENT EMISSION DELIVERY

STUDIU PRIN SIMULARE NUMERICĂ PRIVIND CONSUMUL DE COMBUSTIBIL AL UNUI VEHICUL HIBRID ŞI EMISIILE ELIBERATE ÎN AMBIENT

REZUMAT

Lucrarea prezintă un studiu comparativ de simulare numerică privind economia de combustibil şi emisii al unui vehicul hibrid, atunci când valorile parametrilor temperaturilor respectiv starea de încărcare a sistemului de stocare a energiei sunt alterate şi vehiculul urmează un ciclu standardizat (UDDS). Studiu comparativ are ca şi rezultat folosirea aceluiaşi tip de vehicul, dar cu configuraţie paralelă hibridă, menţinând condiţiile iniţiale.

Key-words: *Fuel efficiency, emissions, UDDS cycle, hybrid electric vehicle – HEV, parallel configuration, state of charge.*

Asist. dr. ing.
Nicolae-Stelian LONTIS
nicolae.lontis@upt.ro

Conf. dr. ing.
Nicolae-Liviu MIHON

Asist. dr. ing.
Ion VETRES

Universitatea Politehnica din Timişoara, B-dul Mihai Viteazu nr. 1, 300222 Timişoara, România

1. INTRODUCTION

In this scientific paper the ADVISOR (Advanced Vehicle Simulator for System Analysis) 2.0 tool will be used to perform the comparison study. Version used for the numerical simulation is 2003-00-r0116. The first version of ADVISOR software was developed and released in November 1994. At the request of U.S. Department of Energy (DOE) for understanding hybrid vehicles behavior, the tool was developed, used later in consultancy and R&D contracts with the automotive big players in that time. The success of the tool developed combined with flexibility and progress, conducted in usage of many other clients in order to assess and understand the system-level interactions of hybrid and electric vehicle components [1].

The ADVISOR tool analyzes vehicle powertrains, focusing on power flows among the components. When used on a model that follows a driving cycle, such as the Federal Urban Driving Schedule (FUDS), its main outputs are fuel consumption and tailpipe emissions. Other capability is to simulate the vehicle in maximum effort acceleration, where outputs are 0-60 mph time or 40-60 mph time, or to determine the maximum road grade the vehicle can climb at constant speed [1]. In accordance with the goals designed, ADVISOR approximates the continuous behavior of a vehicle as a series of discrete steps. During each step, the components are at steady state assumed. This assumption allows the use of efficiency maps or power-usage for the components, derived from steady-state tests in the laboratory. This main assumption is short-duration drivetrain dynamics; however, this not allows investigation in detailed. For example, vibrations in the driveline or oscillations in electric fields is a phenomenon beyond ADVISOR's scope [1]. ADVISOR is an open source license software, developed in MATLAB® /Simulink® environment/graphical program. The program runs under MATLAB® (from 5.2 version on)/ Simulink® (from 2.2 version on), and it can be loaded/started from the command prompt in the

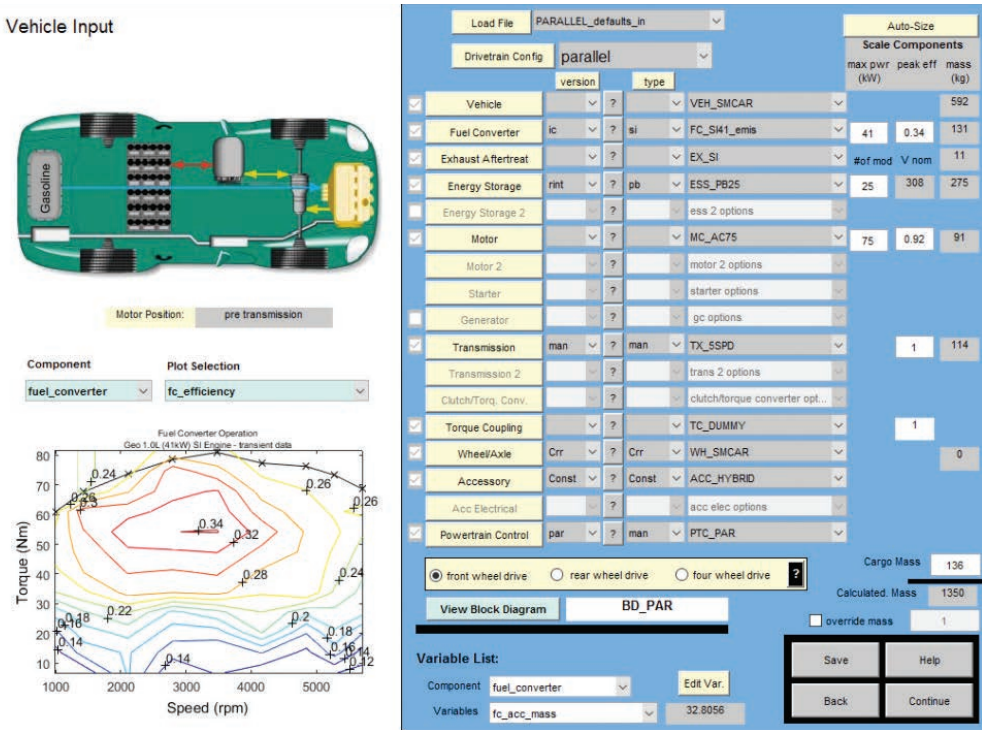

Fig. 1. ADVISOR 2.0 Vehicle Input Screen [2]

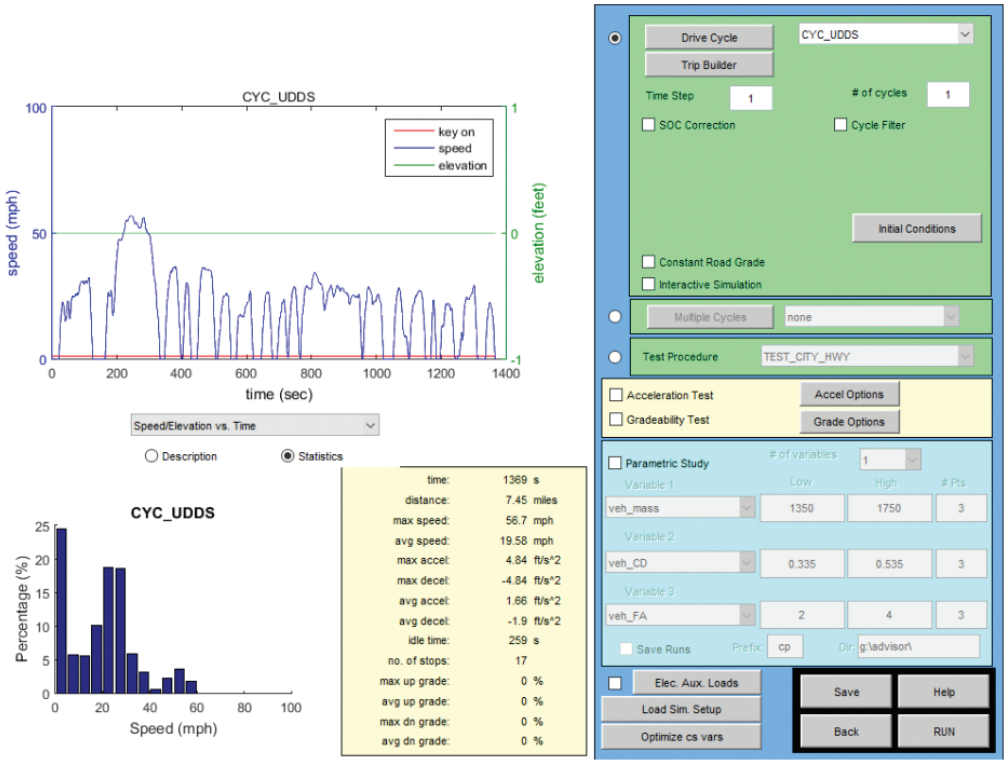

Fig. 2. ADVISOR 2.0 Simulation Setup Screen

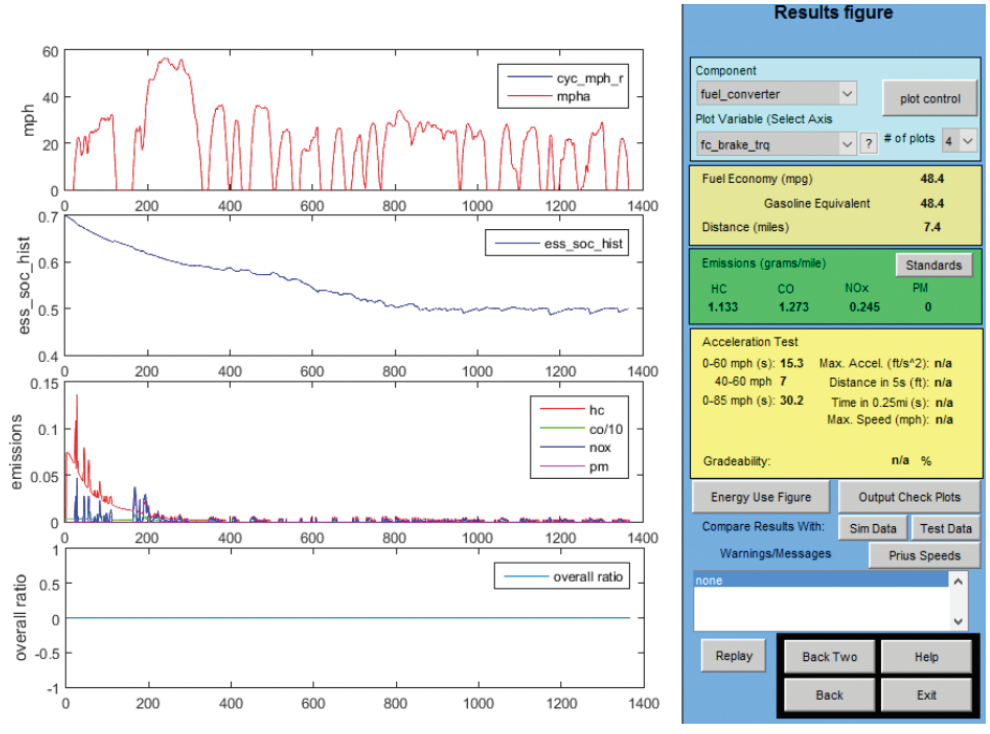

Fig. 3. ADVISOR 2.0 Results Page Screen

MATLAB®/Simulink® software. The simulation tool is composed form three Graphical User Interface (GUI) windows, where the operator can modify certain fields and parameters according to the necessary outputs of the study.

The first GUI presented in Figure 1, is the *Vehicle Input Page* where the operator will introduce the main parameters of the simulation.

The layout of this window is typical for all the 3 GUI windows, in that the left-hand side of the window is the graphical representation of vehicle information; the right-had side is where the user can alter the parameters. On the right-hand side of the window, the user specifies what he wants to see and do to the model (vehicle), and controls the next action for ADVISOR to perform [1].

In Figure 1, vehicle input screen, the picture in the upper left serves as a graphical indication - configuration of the vehicle selected (conventional, series, parallel, fuel cell, or electric vehicle). The user-selectable graphs in the lower left allows the user to view immediately the performance information on the components, that have been selected, such as efficiency lineament for the engine and motor, emissions lineament, and performance graphs for the batteries [1].

On the right-hand side of the vehicle input screen, in the table, the user has control over what type of vehicle is simulated. The user can also replace or add details of all the components (variables) that make up the drive system. Each variable has a pull-down menu that allows different values; selected from the ADVISOR library. The two columns of numbers under the "maximum power" and "peak efficiency" headings initially indicate these values from the data files. Typing in a new number, causes the GUI to linearly-rescale the entire map to match that peak efficiency while preserving the map's original shape. Just above these columns is an "auto-size" knob that simplifies the task of iteratively sizing drivetrain components (engine, motor, and batteries) to meet user-defined minimum performance requirements of acceleration and gradeability. For parallel vehicles, the auto-size function also allows the user to select the degree of hybridization,

Table 1. Ambient setup – parametrization

Variable	Value	Unit [-]	Specification
amb_tmp	20	[°C]	Ambient temperature
air_cp	1009	[J/(kg*K)]	Specific heat of air
ex_cat_mon_init_tmp	20	[°C]	Monolith converter temperature
ex_cat_int_init_tmp	20	[°C]	Internal converter temperature
ex_cat_pipe_init_tmp	20	[°C]	In/out converter pipe temperature
ex_cat_ext_init_tmp	20	[°C]	External converter temperature
ex_manif_init_tmp	20	[°C]	Manifold temperature
fc_c_init_tmp	20	[°C]	Initial temperature of the engine cylinder
fc_i_init_tmp	20	[°C]	Initial engine interior temperature
fc_x_init_tmp	20	[°C]	Initial engine exterior temperature
fc_h_init_tmp	20	[°C]	Initial hood temperature
ess_mod_init_tmp	20	[°C]	Initial temperature of the energy storage system module (ESS)
mc_init_tmp	20	[°C]	Initial temperature of the motor/ controller
ess_init_soc	x†	[-]	Initial state of charge of the ESS

† The initial state of charge of the Energy Storage System will be presumed as 0.00, 0.35 and 0.70, while maintaining the rest of the parameters from initial condition for the Ambient setup with the values presented in the table above.

which reflects the relative sizing of the engine, motor, and batteries [2][3].

The second GUI window of the ADVISOR is the Simulation Setup Page. The primary decision for the user on this screen is whether to run a single desirable cycle or a test procedure, which can consist of special initial conditions, multiple cycles, and significant post processing (such as the test procedure to determine combined city/ highway fuel economy).

In the case of single cycle option, initial conditions (primarily thermal and battery) can be set, and for hybrid-vehicles, the type of battery state of charge (SOC) correction routine is selectable. The two SOC correction options available are a zero-delta or a linear correction routine. The zero-delta routine iterates on the initial SOC until the final SOC is within some tolerance (0.5%), while linear correction routine starts the battery at both its extreme high and low SOC, and then performs a linear interpolation to estimate the fuel economy at the zero-delta SOC crossing. Additionally, evaluation of the gradeability and acceleration is also allowable.

Finally, because parametric studies are often useful to explore the design space of a given vehicle, ADVISOR 2.0 allows the option of

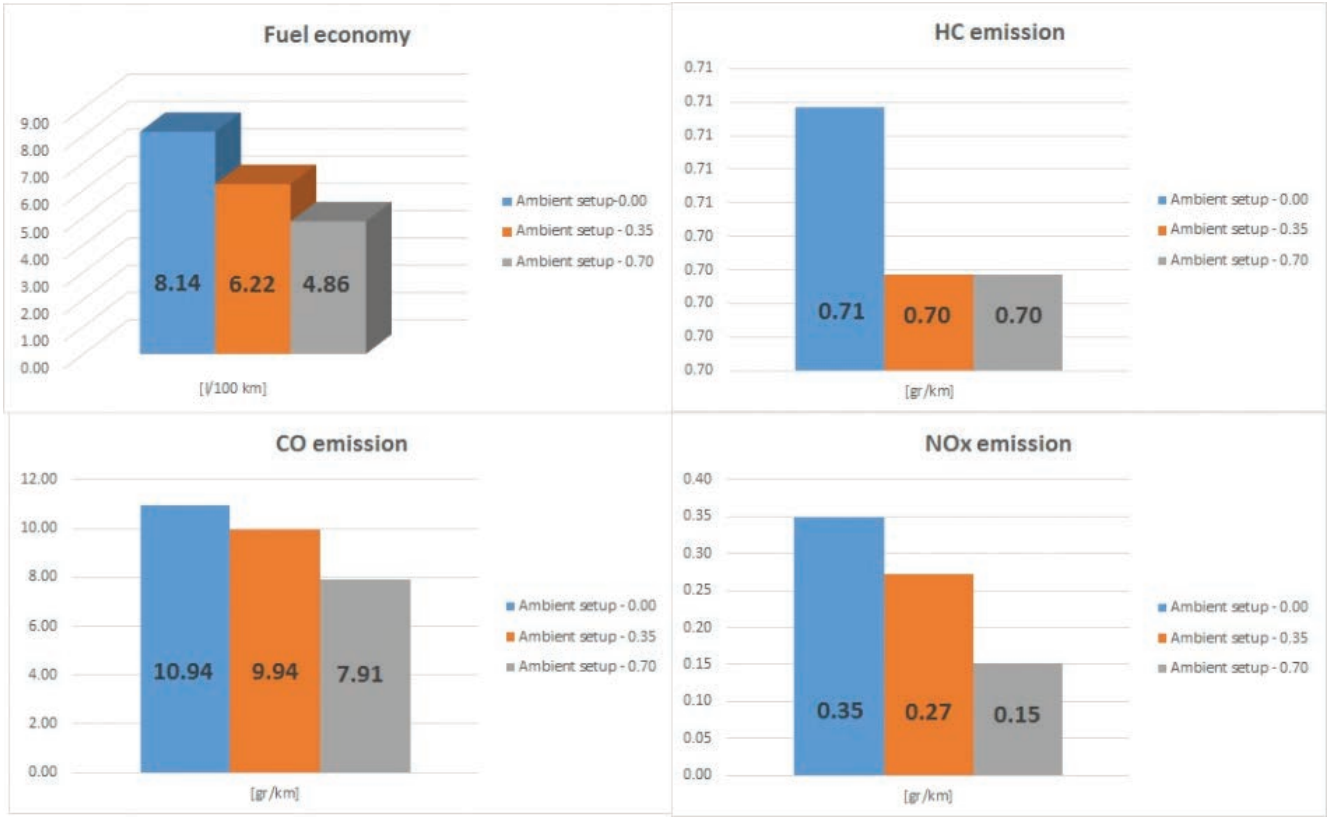

Fig. 4. Ambient setup parametrization results

doing a 1-, 2-, or 3-parameter design sweep of any scalar value on the workspace. This allows the evaluation of the sensitivity of a vehicle to its various input parameters, not only on fuel economy, but also on performance [1][2][3].

The last GUI window of the ADVISOR is the Results Page. The results page presented in Figure 3 allows the user to see the summary results of fuel economy, emissions, acceleration, and gradeability on the right hand side, and plots of any of the time-dependent variables that the tool puts onto the workspace on the left-hand side.

When selecting test procedures rather than single cycles the results screen has separate pop-up windows if. ADVISOR 2.0 allows full usage of the built-in plotting features of MATLAB including zoom, layering multiple curves on the same plots, and applying gridlines.

In Figure 3, which shows a sample Results Screen, it can be seen four plots, chosen as representative plots: vehicle speed, battery SOC, regulated emissions, and temperatures at various places within the exhaust system [4]. Two action buttons pull up an energy usage figure and a series of diagnostic plots. The energy usage figure, tracks all of the energy through the drivetrain, and where it is used performs an energy balance to make sure that there is no unaccounted-for energy. In all windows, is a 'HELP' button that takes the user directly to the online web browser documentation to clarify the upcoming problems.

2. EXPERIMENTAL SETUP

2.1. Model Setup

Model. The model used for comparison test in ADVISOR 2.0 tool is the TOYOTA PRIUS Model powered by internal combustion engine operating in Atkinson cycle, 1.5 l cubic capacity, maximum power 43-kW@4000 rmp, and maximum torque 101 Nm@4000 rpm, correlated with publishing sources, NREL and ANL data. The comparison study starts with vehicle input data (1st GUI); by selecting the PRIUS_JPN_defaults_in model form the Load File knob. For further analysis, basic values of the model are considered.

The next step in the numerical simulation of the Prius model is choosing the condition for the vehicle to run. The proposed driving conditions for the study are UDDS (Urban Dynamometer Driving Schedule) drive cycle. The study will reflect the behavior of the vehicle in terms of: fuel economy (mpg)/gasoline equivalent, distance (miles) and emissions of HC, CO (divided by 10 units), NOx, PM (grams/mile), while the initial conditions (ambient air temperature, specific heat of air, catalytic converter temperature, fuel converter – internal combustion engine/electric engine and engine bay temperature, temperature of the energy storage system (ESS), temperature of the motor/controller and initial state of charge of the ESS) are altered in steps, presuming that the temperature of the systems mentioned above are changing gradually, over one UDDS cycle.

2.2. Result and discussions

The study considered is the vehicle setup describe above and performing the simulation with the initial conditions offered by ADVISOR. Table 1 presents the values selected as initial conditions - ambient setup.

For this experimental setup the initial state of charge of the energy storage system is also altered in three steps (0,00; 0,35; 0,70 – percentage correspondence) while maintaining the values of the numerical simulation parameters constant.

The three situations proposed for the initial state of charge (SOC) for the ambient setup parametrization in terms of fuel economy and emissions revealed as a first conclusion that the optimum condition for driving of the Prius vehicle is with the battery fully loaded. The results

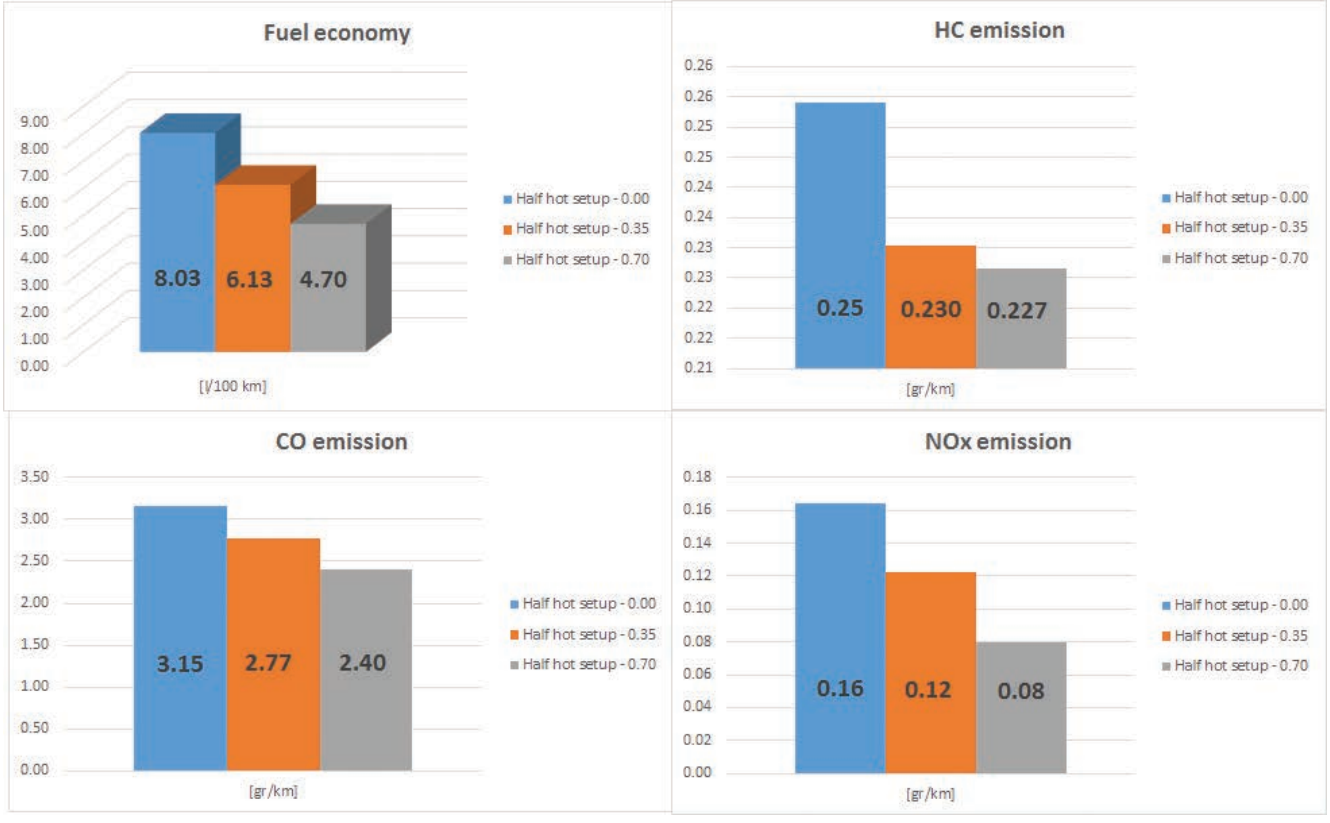

Fig. 5. Half hot setup parametrization results

Table 2. Half hot – parametrization

Variable	Value	Unit [-]	Specification
amb_tmp	20	[°C]	Ambient temperature
air_cp	1009	[J/(kg*K)]	Specific heat of air
ex_cat_mon_init_tmp	250	[°C]	Monolith converter temperature
ex_cat_int_init_tmp	250	[°C]	Internal converter temperature
ex_cat_pipe_init_tmp	150	[°C]	In/out converter pipe temperature
ex_cat_ext_init_tmp	75	[°C]	External converter temperature
ex_manif_init_tmp	150	[°C]	Manifold temperature
fc_c_init_tmp	75	[°C]	Initial temperature of the engine cylinder
fc_i_init_tmp	48	[°C]	Initial engine interior temperature
fc_x_init_tmp	45	[°C]	Initial engine exterior temperature
fc_h_init_tmp	30	[°C]	Initial hood temperature
ess_mod_init_tmp	30	[°C]	Initial temperature of the energy storage system module (ESS)
mc_init_tmp	30	[°C]	Initial temperature of the motor/controller
ess_init_soc	x‡	[-]	Initial state of charge of the ESS

‡ The initial state of charge of the Energy Storage System will be presumed as 0.00, 0.35 and 0.70, while maintaining the rest of the parameters from initial condition for the Half hot setup with the values presented in the table above.

Table 3. Hot setup – parametrization.

Variable	Value	Unit [-]	Specification
amb_tmp	20	[°C]	Ambient temperature
air_cp	1009	[J/(kg*K)]	Specific heat of air
ex_cat_mon_init_tmp	500	[°C]	Monolith converter temperature
ex_cat_int_init_tmp	500	[°C]	Internal converter temperature
ex_cat_pipe_init_tmp	300	[°C]	In/out converter pipe temperature
ex_cat_ext_init_tmp	150	[°C]	External converter temperature
ex_manif_init_tmp	300	[°C]	Manifold temperature
fc_c_init_tmp	150	[°C]	Initial temperature of the engine cylinder
fc_i_init_tmp	96	[°C]	Initial engine interior temperature
fc_x_init_tmp	90	[°C]	Initial engine exterior temperature
fc_h_init_tmp	35	[°C]	Initial hood temperature
ess_mod_init_tmp	35	[°C]	Initial temperature of the energy storage system module (ESS)
mc_init_tmp	40	[°C]	Initial temperature of the motor/controller
ess_init_soc	x§	[-]	Initial state of charge of the ESS

§ The initial state of charge of the Energy Storage System will be presumed as 0.00, 0.35 and 0.70, while maintaining the rest of the parameters from initial condition for the Hot setup with the values presented in the table above.

are presented in Figure 4.

As punctual conclusion it can be observed that when the initial SOC is 0.00, the internal combustion engine has the task to follow the UDDS cycle and also recharge the battery, therefore a higher fuel consumption is experienced, thus resulting higher emissions for HC, CO and NOx.

The same principle was applied in the second case of the numerical simulation when the initial conditions were changed by dividing the hot setup by 2. The parametrization of the simulation is presented in Table 2.

The results of the numerical simulation by altering the parametrization of the initial conditions is presented in Figure 5.

The same trend of decreasing the fuels consumption and emissions is experienced, therefore the usage off the vehicle is recommended to be used like in the previous case, always whit battery fully loaded in order to obtain economy. Another conclusion is that, when the operating temperature of the internal combustion engine was increased the fuel consumption slightly decreased. In terms of emission there is a considerable advantage for this situation, due to the fact that the catalytic converter temperature has increased.

For the third numerical simulation setup, was proposed the hot setup parametrization (in table 3 are presented the values of the simulation parameters), a default situation that the simulation software provides, when it is appealed.

The results, presented in figure 6, conclude that the decreasing trend of the fuel consumption and emissions occurs, when the temperature of the internal combustion engine and catalytic converter is optimal.

Comparing the results for the fuel consumption, for the three numerical simulation parametrization and three initial SOC, it can be attested that the an average of 0.17 l/100 km of fuel is saved, for the first case

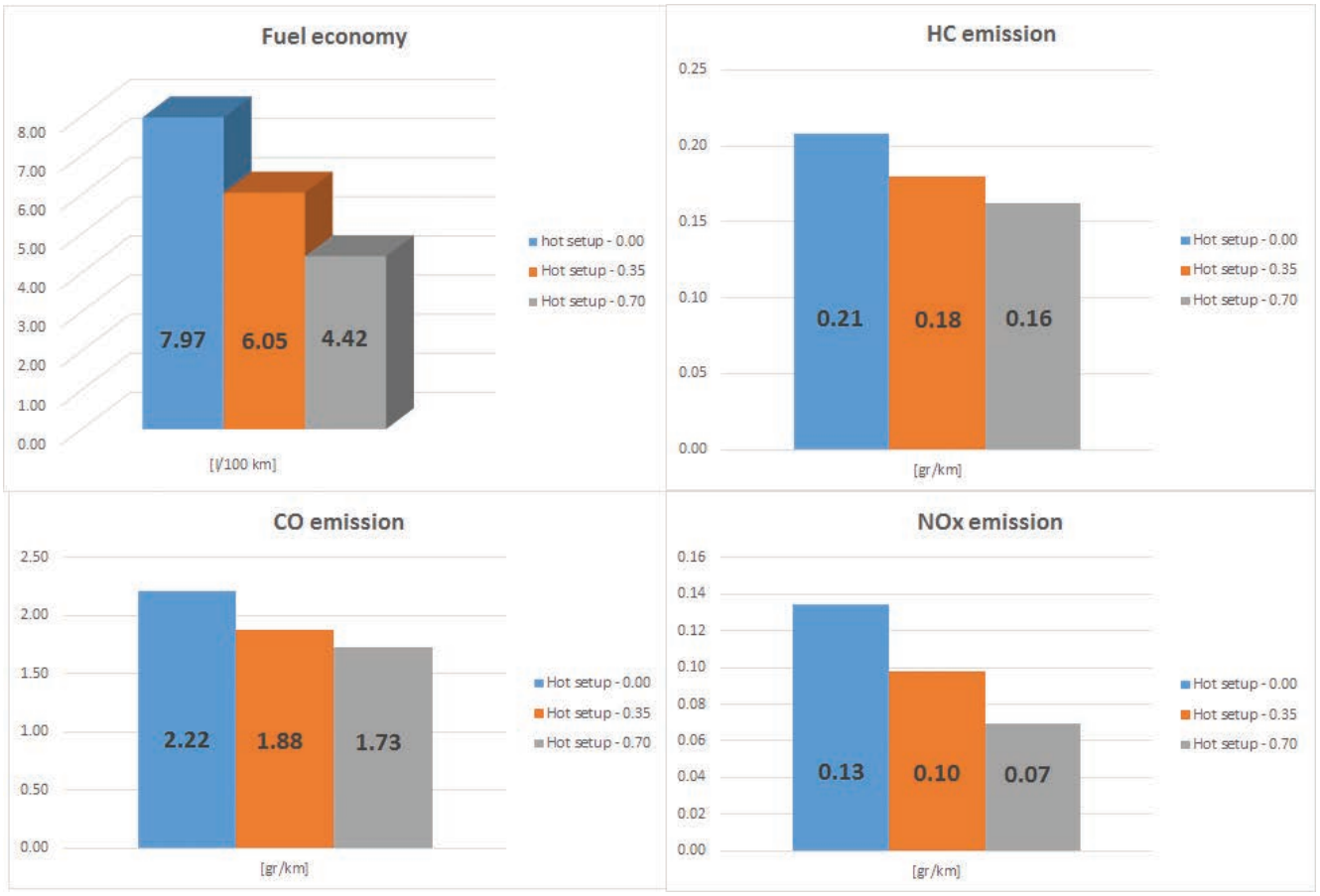

Fig. 6. Hot setup parametrization results

(ambient setup / hot setup parametrization and initial SOC 0.00 / 0.35).When the initial SOC is increased – translated to fully battery charged when starting the vehicle and diving on the UDDS cycle – the fuel economy is increased by 0.44 l/100 km.

Regarding the HC emissions in the first setup parametrization – ambient consideration, the values are the same for every initial SOC value; in other words the vehicle in cold state can be driven in any situation (battery full or discharged), the HC emission remaining the same. When the parametrization is changed and the second and third step occurs, the temperature of the catalytic convertor increases and the emissions are apprehended. The difference is more than 50% less HC emissions comparing to the second case of parametrization (half hot – setup), and even more decreases when the hot setup is performed.

The Carbon Monoxide emission is dramatically reduced when the temperature of the catalytic converter is increased, and continuous to decrease when the initial SOC is also increased; in average the gain of carbon monoxide emission is approximately 80 %.

For the NOx emission, the gain is lower than in the case of CO, but considerable taking into account that the average value is approximately 50% less the ambient setup parametrization in comparison with the second and third situation.

3. CONCLUSION

One global conclusion of this study reflects the fact that, when the hybrid vehicle is used as a mean of transportation, certain obligations of the driver/owner of the vehicle emerges. The first obligation is that the driver has to connect the vehicle to the power grid when the vehicle is stationary (newer Toyota Prius Model), or check permanently the SOC indicator of the vehicle, in case the fuel economy and emissions decrease is a priority.

Another conclusion of the present study in this paper is that the vehicle has a good behavior when is operated at optimum temperature, therefore is prolific for it when is used as a door to door service provider.

Lucrare prezentată în cadrul Congresului Internațional de Inginerie a Autovehiculelor și Transporturilor - CONAT 2016, 26.10 – 28.10.2016, Brașov, România, și publicată în Proceedings of the Congress (ISSN 2069-0401).

REFERENCES:

[1] Advisor 2.0: A Second- Generation Advanced Vehicle Simulator for Systems Analysis – NREL/TP-540-25928 Technical report (March 1999)

[2 Markel, T., Brooker, A., Hendriks, T., Jhonson, V., Kelly, K., Kramer, B., O'Keefe, M., Wipke, K.: *ADVISOR: A system analysis tool for advanced vehicle modeling*, Journal of Power Sources, Volume 110, Issue 2, 255 – 266 (2002)

[3] Wipke, K.B., Cuddy, M.R., Bruch, S.D.: ADVISOR 2.1: *A user-friendly advanced powertrain simulation using a combined backward/forward approach*, IEEE Transaction on Vehicular Technology, Volume:48, Issue:6, (1999)

[4] Gao, D.W., Mi, C., Emadi, A.: *Modeling and Simulation of Electric and Hybrid Vehicles*, Proceedings of the IEE (Volume: 95, Issue: 4 (2007)

[5] Advisor 2.0 Software version 2003-00-r0116

[6] http://www.epa.gov/nvfel/testing/dynamometer.htm

ANALYSIS OF THE CAR BODYWORK PROTECTIVE COATING'S DESTRUCTION IN CONTACT WITH MARINE BIRD DROPPINGS ON THE BLACK SEA COAST

ANALIZA DISTRUCȚIILOR ACOPERIRILOR CAROSERIEI AUTOVEHICULELOR LA CONTACTUL CU EXCREMENTELE PĂSĂRILOR MARINE ÎN ZONA LITORALĂ A MĂRII NEGRE

REZUMAT

În lucrarea prezentată se pune in evidență posibilitatea de a identifica, pe baza unui "șablon vizual determinat", distrucțiile acoperirii caroseriei autovehiculelor la contactul cu excrementele păsărilor marine în zona litorală, explicitându-se - cu referire directă asupra unui element de caroserie al unui tip și producător din clasa premium, prin raportare referențială și măsurători sistematice de precizie (a grosimii stratului de acoperire în zona afectată, forma deformației stratului de acoperire simulată în mediu virtual, temperaturii caroseriei relativ la variațiile temperaturii mediului), cu evidențierea eventualelor cauze ale pierderii calităților estetice și de protecție a acestuia.

Key-words: *Automotive body coating layer, destructions caused by external factors on automotive coating frame, factors favoring the destruction of the coating, visual pattern effect on bird droppings over the car-body-frame coating film layer destruction.*

Prof. dr. ing.
Laurențiu-Claudiu MANEA
profmanea@yahoo.com

Prof. dr. ing.
Adriana-Teodora MANEA

Drd. ing.
Camil TUDOR

Universitatea "Ovidius" din Constanța, Bulevardul Mamaia, Nr. 124, 900001 Constanta, Romania

1. INTRODUCTION

This research is the subject of a Court case in which the owner request replacement of his new vehicle during warranty period, because of changing of its premium range car aesthetics outer coating bodyframe panel left rear wing-. Technical expertise had to determine either the distruction was due to alleged causes generated by the production process of the manufacturer, or there were prerequisites for a destructions caused by external factors – in case - those which appear in contact with the droppings of seabirds in the marine coast aria -. Finally we find a similarity with a recognised distruction pattern, already noticed by the specialists, for this type of the external factors impact over the protective coating film of the car frame.

2. EXPERIMENTAL MEASUREMENT AND SIMULATION IN VIRTUAL ENVIRONMENT OF THE COATING OF BODY PARTS IN QUESTION

Visual analysis carried out on the state of body coverage (with multiple layers which include color pigment layer - and final transparent protective layer -) shows that in the area of interest investigated in the aesthetic destruction signaled was made a strong polishing action with a rotary device, without the removal of the reported deficiency (Figure 2 a, 3).

Taking a set of measurements in the area of interest with metrologised equipment supplied, after statistical and mathematical experimental data processing we can see that there are two types of mechanical stress applications of the coating framework panel „left-wing rear-area B: points 13,14, 15, 16, 25 are in a „depression" relative to points 8,10,19, on the same level with 19, as the area around the depression as „up" over a toughest element of stability that would be at the center of it. (Areas colored dark red to indicate this izo-height curve located at the points 17, 18, 9), the differences being (on average order) of 5-7 microns Because the research area in question -B, Figure 1, turned out to be, after the measurements made between the right similar body panel, with reference to left body element from the carframe of 2016 production time (with an Aluminium and not ferrous frame) coverage area uneven lower than in areas adjacent (probably part because of technology coverage on the painting manufacturer's plant, either possible in our opinion due to the emergence unauthorised effort applied on the protective surface by strong polishing -hoping uniform the final transparent coating film surface at the site - (Figure 2 a2,3 - obvious circular destructions show in polarized light). We had to observe that the final thickness of the coating measuring of the body was within the limits stated by the manufacturer. After the panel surface of the left rear wing was digitized with MATLAB software we „virtualy zoom in" the affected area (Figure 1 B-zone, bounded by the measuring points 9,10,11,18,12,25,13,14,15,16 - corresponding to the measurement values of the coating thickness), to establish a „template or a pattern" deformation, and later, to compare it with the related assumptions and existing cases in the bibliography in order to move forward and argue a possible succession of emergence and evolution of the destruction. (Figure 3).

2.1. Analysis of the experimental measurements results

Summarizing the observations, emerge the following assumptions validated by the experimental measurements:

1. The damage appeared likely in the summer time season in 2015 when there were above normal maximum elevated temperatures during the day on the Constanta Black Sea Coast (33-35 degrees C), and when the at black color body exposed to direct sunlight reached very high temperature values (60-80 degrees C) due to strong caloric radiation absorbing [6].
2. Exists on the damaged area izoheights divergent type „depression" (at 10 microns scale) generated either by a corrosive attack on the transparent coating or due to a change (within 7-10 microns) in the surface layer of the transparent and color film in still uncertain circumstances;
3. Exists on the body panel „ back wing „ so on the vehicle in question and also on the reference dealer's vehicle a reduction measured of the coating in the area where there was reported the damage (but currently in the technological limits indicated by the manufacturer) due probably either of the

a. Left rear wing of the car in case, viewing on B zone - area under further „zoom"virtual measurements investigation

b. 2016 metrologised & quality control meter gauge used during mesurements

Fig. 1. Technical aspects of obtaining experimental measurements of coating thickness distribution on framepanel „rear wing" in zone B

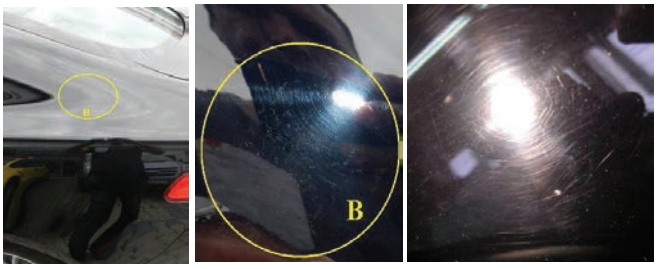

a. in relation with paintwork coating damages; Area B-Figure 1

b. zoom on „spider type template" area B - under investigation

Fig. 2. Photos of the claimed aesthetic damaged area of the left rear wing body panel

surface shape or constructive design configuration panel of body frame „rear wing" either or because of the technology painting (grain drop paint, tilt head robot painting, instantaneous pressure design particle paint cone, value of the electrostatic field created between body and „ground"), the total thick coverage remain more consistent towards the upper edge of the body „rear wing" and less in zone B, - where the present claim and research was focuses. It should be added that coating, if studied (when the coating thickness was not influenced by -repair coatings, paints, and subsequent transparent coatings-) falls within the general engineering supported documentary producer, between 79 microns and 526 microns.

4. Since the relevant experimental data reveal that in the B area from Figure 1 has been shown to be measurements with uneven horizons of izoheights lower than adjacent areas it is possible that this highlight the damages made by an unauthorized polisher in his effort of clearing and uniform the coating damaged surface – Figure 2.a,2,3, (evident transparent coating circular destructions –in polarized light /n.r.);

5. It is likely that once damaged the paint and the varnish, either from technological or from external reasons (through its removal by an unauthorized intervention) to be amplified the initial destruction, whereas in the polarized light zone we can clearly observe „circular grooves" resulting from unauthorized polisher or likely improper abrasive grain based on chromium (Figure 2.a).

Along with recommendations (shown in Figure 4) may not respected by the owner in this regard, research has identified on the manufacturer's official website a set of recommendations related to the maintenance of the body, which in part included in the present maintenance manual of the car.

As alongside the repeated operation of polish (for protection coating of the bodywork) which had to be done only by qualified personnel, with polish cream recommended only by the dealer of the producer (without abrasive particles based on chromium) and additional textile materials agreed by the brand, the recommendations for maintenance on body surface coatings have strong indications upon „aggressive and corrosive attack of bird droppings", given that on the Black Sea Coast there are many species of marine birds that usually random defecates we started also the search in this direction, linking it with the related observations of specialists in marine biology that claims the increased acidity content of birds excretory system (concentrating in one place called „vent" - liquid and solid manure). Studies show that marine bird droppings (which varies depending on the species, diet, season) are a cocktail composed of salts rich in nitrogen (8-16%), ammonia, ammonium oxalate, urate, uric

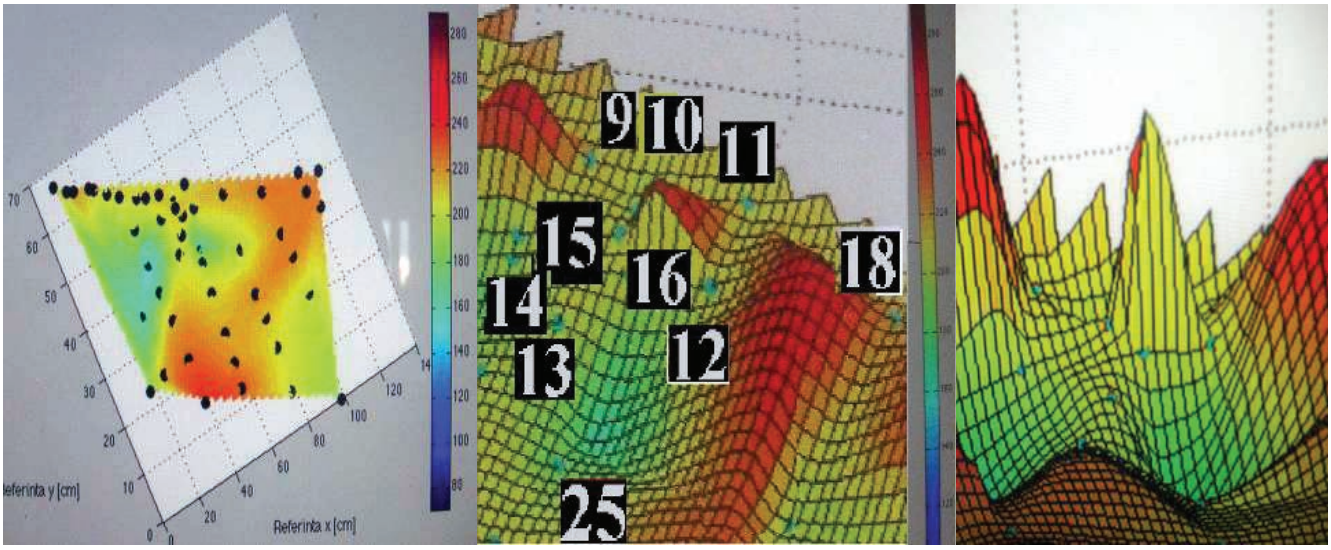

a. car left rear wing –in the case- with B –figure 1 under investigation area (visualization with virtual magnifiing „zoom")- Mathematical distribution defined by the measuring points 9,10,11,18,12,25,13,14,15, 16, 25 and experimental results in terms of coating thickness analysis -inside manufacturer limits-
Fig. 3. Issues getting through virtual simulation in MatLab of the coating thickness on the frame panel „rear wing" B area

phosphate, uric acid and phosphoric potassium (2-3%) / ammonium biological materials, including bacteria and enzymes [4] and that the oil contained in the excrement of seabirds make their adhesion to automotive paint to be big and have the effect of catalyzing attack reactions on cover frame body coating films.

A research laboratory sample of the body panel requested by the technical expert (not accepted by car owner who desire to preserve evidence for future expertise), (heated to 60-80 degrees C, in reaction with the mix of these components from sea bird droppings and then cooled to a difference of 45-60 degrees C levels, could provide useful information about behavior of the coatings layer's coverage on in these circumstances, of course respecting ISO 2812-5: 2007 Figure 6 –coatings, varnishes - determination of resistance to liquids - part 5: temperature-gradient oven method where specified a method of determining the resistance of the coating material to the action liquid or semi-liquid, variant simulation -with bird droppings diluted with water-pancreatic would allow the application of ISO 3696 „water analytical laboratory use - specifications and test methods" being not applicable) Studied bird droppings in contact with the car body coatings proved harmful varnish and paints damages, fading and even in depth degradation of the bodywork coverage (Figure 2), amplified by:

1. magnifying to time reaction (destruction can occur within a few hours of action, so it is extremely important to made a rapid removal of the deposits from the surface of the car-body). Deposits must be removed as soon as possible with a solution agreed by the manufacturer (which is usually based on distilled water and isopropyl alcohol and other constituents in well established proportion) which must be allowed to react on the deposit more than 10 minutes on a piece of fabric agreed -as in addition to the corrosive effect there are many biological materials with severe impact on human health „so cleaning hands is strongly advised or carried out only with special gloves protection."
2. grain excrement and water content (as the grain deposit is bigger it becomes more rigid during the day and during the night on the cooled the body, if it is not removed, it becomes solid so the inflated transparent film of varnish and paint around shrinks around it taking the form of a cone or a „spider webs" as it is considered in the literature: „typical damage attack pattern to the car body coating with bird droppings" (see Figure 1 versus Appendix 1).; the water content maximizes grip and manure to activate the reaction body shell leveraging it in the early stages, until the formation of solid deposit.
3. temperature of the car frame during the impact (leading to the

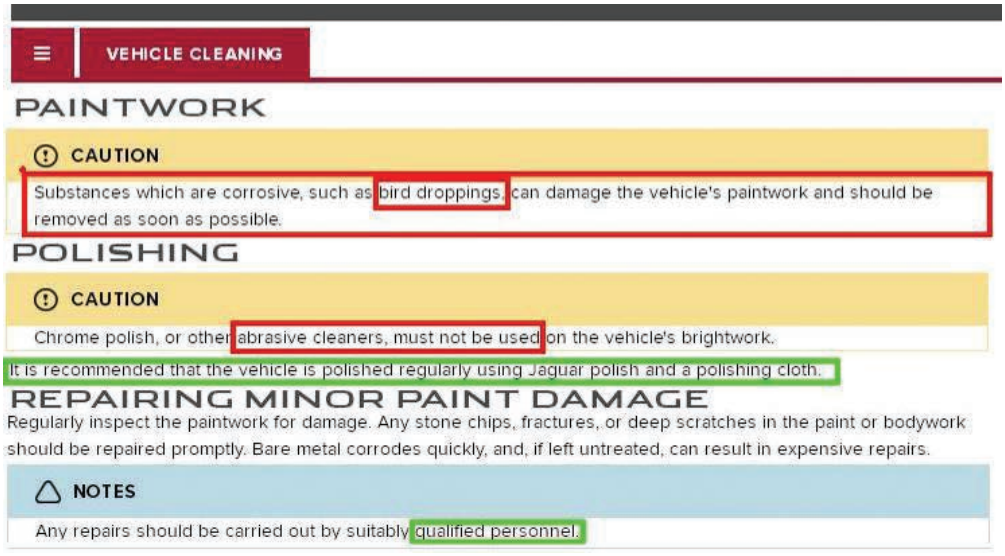

Fig. 4. Owner obligation to respect producer's rules related with the maintenance of body frame paint-coating

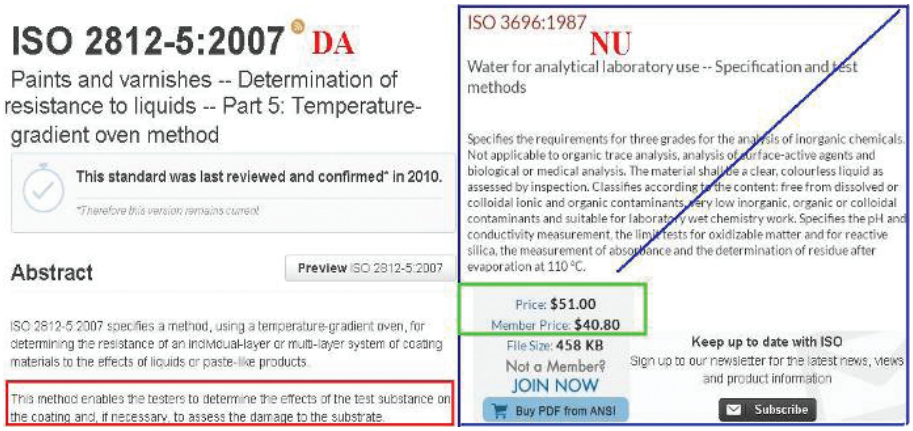

Fig. 5. Standards ISO 2812-5: 2010 to be applied in laboratory in case of an attack of various substances on multilayer coatings

activation of components in the coating layer dilated and attack deeper and more corrosive the varnish layer stretched on smaller inflated thickness, and dry faster and intense deposit solid. Dark colors of bodies are most exposed (black amassing maximum heat radiation) and high temperatures during hot summer days amplifies the destruction process (see Figure 5);

4. high temperature variation on hot summer days versus night, with daytime maximum temperatures exceeding 30 degrees C and 16-23 degrees C during night time, cause dilation and extent of the clear coat and the paint during the day, and in the event of a deposit which rapidly solidifies contraction of different paint around the varnish and with specific destructions of the paintwork with color pigment. If the reaction persists then cause irreversible damage to the protective layer of varnish and repainting it is necessary on the entirely body part.

5. Thickness of the multi surfaces coatings with producer technological limits from 79 to 526μm offers a very extensive thickness coating interval; measurements on the vehicle body in the case (also on the dealer's reference one) generally indicated that values are within the specified limits but in the interest area (zone B-Figure 1) it was proven experimentally a local decrease of the coating thickness film. We had not at our disposal a powerful laboratory device to measure the thickness of each distinctive layer deposited in that area but we presumed, from the technological specifications, that it is expected to be in the same thickness proportion over the entire body. This shows that the area B, with a proven thickness less substrate (which expands at high temperature thinning further its thickness) may be more susceptible to an attack with more persistent and more evident destructions than other areas of the car-frame.

6. The thickness of the body and its position in relation to the sun prior to the impact with the corrosive substance. The element body is exposed to sunlight (top left rear wing). The related image's documentation available in the bibliography and in other video and photo documents from the Internet (whose content vas selectively presented in Appendix 1), show that the interaction of bird droppings over the covering film coating of a car body resulting can be compared with a form of destruction or „a pattern - spider web type -" as the the owner of the car in question complained on]n the court relating with its left rear wing (Figure 2 b) damage. In this stage we can advance the following observations:

1. Architecture (design and organization) claimed the overall destruction of „spider web" on the paintwork with color pigment under the transparent layer of lacquer is similar to those identified as „follow the dung-bird droppings -type" on its own coating layer premium car body frame.

2. We can not compare the magnitude of destruction „in deep" because no producer technical data were provided for comparison in this respect and for the car in the case is considered that the not conform polishing treatment destroy the margins of the affected area and made irrelevant a microscopic laboratory search of the damaged coating film „in situ".

3. CONCLUSION

Studied bird droppings in contact with the car body coatings have been proven harmful for varnish and paints, causing fading and even degradation in depth the film coverage of the bodywork (Figure 2 versus Appendix 1) effects amplified by: maximizing the time of reaction (destruction can occur within a few hours of action, so it is extremely important to remove rapidly the deposits from the surface of the body), grain, manure and water content there of (as the grain is bigger the deposit becomes more rigid and if it not removed during the night cool of the frame, it becomes a solid around which clear coat and paint shrinks, the paint taking the form of a cone or a „spider webs" . One it consider as a „typically damage attack of bird droppings on car frame /see Figure 2) „body temperature during the impact, body color, the thickness of the coating film of the car-frame, thickness of the frame panel and its positioning in relation to the sun (prior to the impact with the corrosive substance);

We can say that in the respect of our search exist the possibility of finding a corresponding „pattern of destruction" type-like „image of spider webs" contraction of the color paint film under the protective transparent car-frame coating.

ACKNOWLEDGEMENTS

The authors want to thanks to Mr. Barbes I from the Petromidia Petrochemical Refinery Plant, Technical measurements Laboratory that putted to our disposal the measuring gauge, and also to Mrs. Cristina Manea, who use hers knowledge in MatLab programming software to define the coating surface of the vehicle's body frame.

Lucrare prezentată în cadrul Congresului Internațional de Inginerie a Autovehiculelor și Transporturilor - CONAT 2016, 26.10 – 28.10.2016 Brașov, România, și publicată în Proceedings of the Congress (ISSN 2069-0401).

REFERENCES:

[1] Hutchinson, G.,E., *Survey of contemporary knowledge of biogeochemistry*, Bulletin of American Museum of Natural History, volume 96-554, 1950.
[2] Williams, D., The Telegraph 6:30AM BST 10 May 2011 http://www.nissan-global.com// Researches of Auto Glym
[3] Dave, K.,G., *Machine polishing by rotary polisher*, www.Detailingword.co.uk
[4] Thornton, J. I., *Forensic Paint Examination*. In Forensic Science Handbook, 2nd ed.; Saferstein, R., Ed. Prentice Hall: Upper Saddle River, NJ, 2002; Vol. 1, pp 429-475. 4. Standard Guide for Forensic Paint Analysis. In 02, E.-. Ed. ASTM International: 2002.
[5] Streitberger, H. J., & Dossel, K. F. (2008). *Automotive paints and coatings*. John Wiley & Sons
[6] www.webimage.ro
[7] www.wunderground.com/history

GEOMETRIC CONSTRAINTS AT THE VALVE ACTUATION MECHANISM WITH SPHERICAL CONTACT BETWEEN THE LEVER AND THE HEAD OF THE VALVE

CONSTRÂNGERI GEOMETRICE PENTRU UN MECANISM DE DISTRIBUȚIE CU CONTACT SFERIC ÎNTRE CULBUTOR ŞI CAPUL SUPAPEI

REZUMAT

În lucrarea de față se stabilesc relațiile geometrice care trebuie să fie satisfăcute datorită contactului sferic dintre diferite elemente ale unui mecanism de distribuție. Cu ajutorul acestor relații se poate determina unghiul de rotație al culbutorului în funcție de restul parametrilor, precum și unghiul maxim de rotație în funcție de poziția dintre culbutor și supapă. Teoria este evidențiată cu ajutorul diverselor diagrame de variație.

Key-words: *Valve-lever contact, geometric relations, rotation angle*


Prof. dr. ing.
Nicolae-Doru STĂNESCU[1]
s_doru@yahoo.com


Drd. ing.
Ionuț DRAGOMIR[2]


Prof. dr. ing.
Nicolae PANDREA[1]


Conf. dr. ing.
Adrian CLENCI[1]


Prof. dr. ing
Dinel POPA[1]

[1] Universitatea din Pitești, Str. Targu din Vale, Nr. 1, 110040 Pitesti, Romania
[2] AKKA ROMSERV, Bucharest, Romania

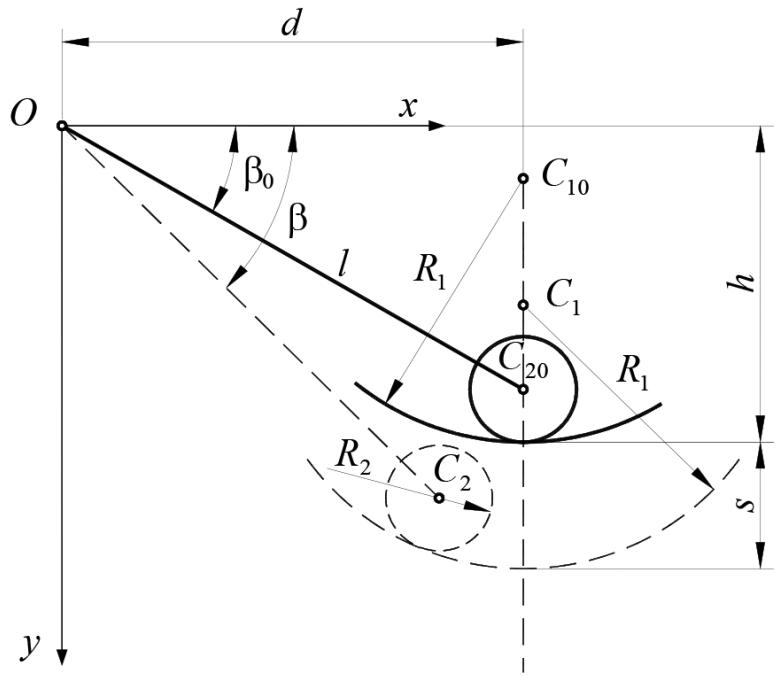

Fig. 1. The mechanical system

1. INTRODUCTION

The problem of the valve actuation mechanism with different type of contact between the cam and tappet, and between the lever and the head of the valve is of great importance in the field of automotive. Different types of cam-follower mechanisms are studied in the literature [1]. Some of the modern automobiles use now roller tappet mechanism and spherical contact between the lever and the head of the valve. The general synthesis of a distribution mechanism with general contact curve is described in [2]. The problem of a continuously variable valve lift mechanism from the point of view of the analytical synthesis and kinematic analysis is discussed in [3]. The general method used in the cam synthesis may lead to singularities which may cause failures in functioning. A new method to obtain convex cam is to use the Jarvis march which assures the convexity of the cam [4]. The study of such mechanism leads to complicate formula and the determination of different parameters that appear in these formulae cannot be made in an analytical way. For these reasons a numerical solution must be given. In addition, the accuracy of the results is obtained using a very small scale (in our paper we used a precision of 10^{-13}, that is, the solving of the non-linear systems obtained in the paper is performed until the absolute value of the function is less than this value). Moreover, the derivatives of the rotations angle in function of the rotation angle of the crankshaft have to be determined using the theory of the implicit functions. These derivatives will be developed in another paper in which we will discuss the synthesis of the cam mechanism. Based on the previous considerations, we have drawn some diagrams which present the variations of the rotation angle as function of different other parameters.

2. DESCRIPTION OF THE SYSTEM

The considered system (Figure 1) consists in the bar (which symbolizes the lever) OC_2 having the length equal to l, and having at its end a roll of radius R_2. In the initial position the angle between the bar and the

horizontal direction is equal to β_0, which is known. The rotation of the valve about its own axis of symmetry is a redundant degree of freedom which is not important in our analysis. For this reason, the problem may be considered a planar one and the sphere-sphere contact is presented as a contact between two circles situated in the same plan. The physical realization of the contact uses two spheres because the elimination of the rotation of the valve is a complicate task, and this rotation is wished from the point of an uniform wear of the lever and valve.

The roll of radius R_2, supports at any moment of the motion, on an arc of circle of radius R_1; the center of this circular arc is situated at the distance d from the vertical axis O_y.

We may write the relation:

$$d = l\cos\beta_0 \tag{1}$$

The displacement of the valve in vertical direction with the distance s leads to the displacement of the circular arc of radius R_1, so that the center C_1 of this arc moves from the position C_{10} to the new position C_1, but remaining situated at the distance d from the axis O_y.

The bar of length l rotates such that the roll of radius R_2 remains tangent to the circular arc of radius R_1, while the angle between the bar OC_2 and the axis O_x takes the value β.

The systems must assure a required maximum displacement of the valve, s_{max}. This value is necessary for a good intake of the fuel in the cylinders

3. GEOMETRIC CONSIDERATIONS

The coordinates of the point C_2 (the center of the roll) read

$$x_2 = l\cos\beta \qquad y_2 = l\sin\beta \tag{2}$$

The circle of center C_1 has the equation

$$(x - x_1)^2 + (y - y_1)^2 = R_1^2 \tag{3}$$

where x_1 and y_1 are the coordinates of the center C_1,

$$x_1 = d \qquad y_1 = h + s - R_1 \tag{4}$$

The equation of the circle of center C_2 and radius R_2 has the form

$$(x - x_2)^2 + (y - y_2)^2 = R_2^2 \tag{5}$$

The intersection point of the two circles is obtained as the solution of the following system

$$\begin{cases} (x - x_1)^2 + (y - y_1)^2 = R_1^2 \\ (x - x_2)^2 + (y - y_2)^2 = R_2^2 \end{cases} \tag{6}$$

Subtracting the two equations (6), term by term, one obtains the relation

$$(2x - x_1 - x_2)(x_2 - x_1) + (2y - y_1 - y_2)(y_2 - y_1) = R_1^2 - R_2^2 \tag{7}$$

where from it results the expression

$$2(x_2 - x_1)x + 2(y_2 - y_1)y = R_1^2 - R_2^2 + x_2^2 - x_1^2 + y_2^2 - y_1^2 \tag{8}$$

Denoting

$$A_1 = 2(x_2 - x_1), \quad B_1 = 2(y_2 - y_1), \quad C_1 = R_1^2 - R_2^2 + x_2^2 - x_1^2 + y_2^2 - y_1^2 \tag{9}$$

the expression (8) becomes

$$A_1x + B_1y = C_1 \tag{10}$$

where from

$$y = \frac{C_1}{B_1} - \frac{A_1}{B_1}x \tag{11}$$

Replacing now in the first relation (6), one gets

$$(x - x_1)^2 + \left(\frac{C_1 - A_1x}{B_1} - y_1\right)^2 = R_1^2 \tag{12}$$

expression which leads to the equation

$$x^2 + \frac{A_1^2}{B_1^2}x^2 - 2xx_1 - \frac{2A_1(C_1 - B_1y_1)}{B_1^2}x + x_1^2 + \left(\frac{C_1 - B_1y_1}{B_1}\right)^2 - R_1^2 = 0 \tag{13}$$

With the aid of the notations

$$A_2 = 1 + \frac{A_1^2}{B_1^2}, \quad B_2 = -2x_1 - \frac{2A_1(C_1 - B_1y_1)}{B_1^2}, \quad C_2 = x_1^2 + \left(\frac{C_1 - B_1y_1^2}{B_1}\right)^2 - R_1^2 \tag{14}$$

the expression (13) may be put in the form of a second degree equation

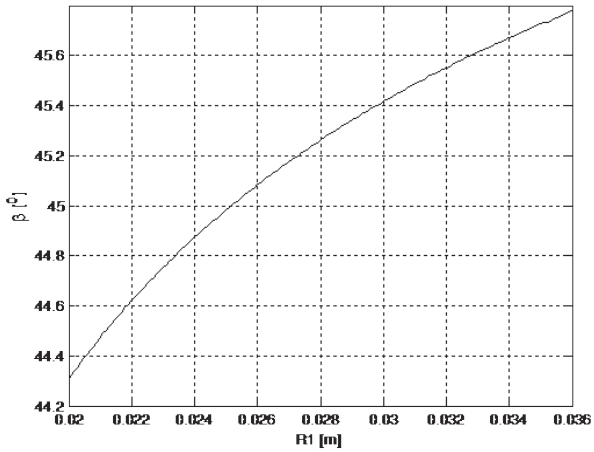

Fig.2. The variation $\beta=\beta(R_1)$

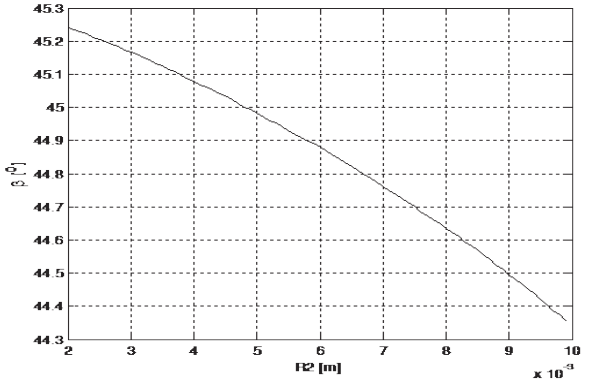

Fig.3. The variation $\beta=\beta(R_2)$

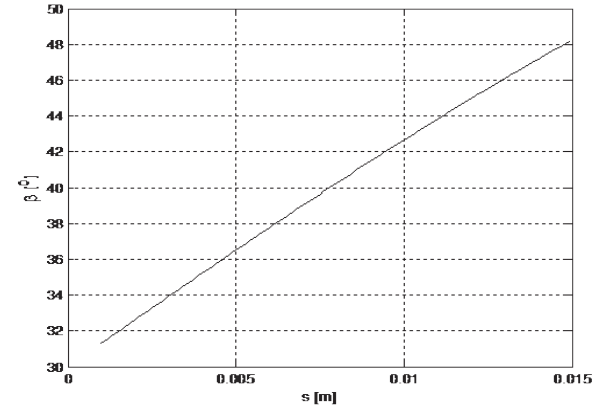

Fig. 4. The variation $\beta=\beta(s)$

in the unknown x,

$$A_2x^2 + B_2x + C_2 = 0 \tag{15}$$

The tangency condition of the two circles implies that the equation (15) has a unique solution in the unknown x, that is, its discriminant vanishes,

$$\Delta = B_2^2 - 4A_2C_2 = 0 \tag{16}$$

Keeping into account the relations (2), one successively obtains

$$A_1 = 2(l\cos\beta - x_1), \quad B_1 = 2(l\sin\beta - y_1), \quad C_1 = R_1^2 - R_2^2 + l^2 - (x_1^2 + y_1^2)$$
$$A_2 = 1 + \left(\frac{l\cos\beta - x_1}{l\sin\beta - y_1}\right)^2, \quad B_2 = -2x_1 - \frac{(l\cos\beta - x_1)\left[R_1^2 - R_2^2 + l^2 - (x_1^2 - x_2^2) - 2(l\sin\beta - y_1)y_1\right]}{(l\sin\beta - y_1)^2} \tag{17}$$

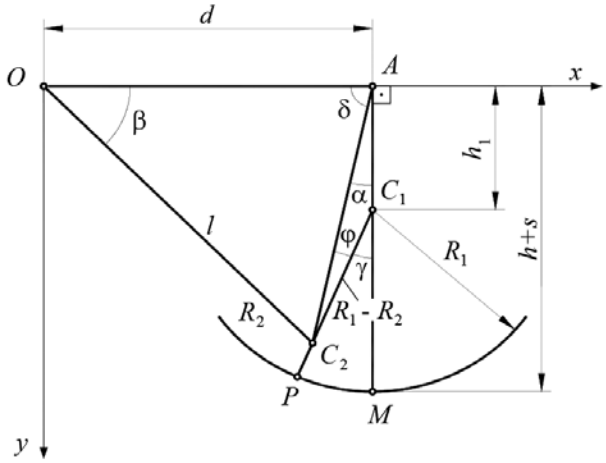

Fig. 5. The geometric schema

$$C_2 = x_1^2 + \left[\frac{R_1^2 - R_2^2 + l^2 - \left(x_1^2 + x_2^2\right) - 2(l\sin\beta - y_1)y_1}{2(l\sin\beta - y_1)}\right]^2 - R_1^2 \tag{18}$$

We denote

$$A_3 = R_1^2 - R_2^2 + l^2 - \left(x_1^2 + y_1^2\right) \tag{19}$$

and we get

$$A_2 = \frac{l^2 + x_1^2 + y_1^2 - 2lx_1\cos\beta - 2ly_1\sin\beta}{(l\sin\beta - y_1)2}, \quad B_2 = \frac{-2x_1(l\sin\beta - y_1)^2 - (l\cos\beta - x_1)[A_3 - 2(l\sin\beta - y_1)y_1]}{(l\sin\beta - y_1)^2}$$

$$C_2 = \frac{4x_1^2(l\sin\beta - y_1)^2 + [A_3 - 2(l\sin\beta - y_1)y_1]^2 - 4R_1^2(l\sin\beta - y_1)^2}{4(l\sin\beta - y_1)^2} \tag{20}$$

The equation (16) becomes now

$$\begin{aligned}&\left\{2x_1(l\sin\beta - y_1)^2 + (l\cos\beta - x_1)[A_3 - 2y_1(l\sin\beta - y_1)]\right\}^2 \\ &\quad - \left(l^2 + x_1^2 + y_1^2 - lx_1\cos\beta - 2ly_1\sin\beta\right) \\ &\times \left\{4x_1^2(l\sin\beta - y_1)^2 + [A_3 - 2y_1(l\sin\beta) - y_1]^2 - 4R_1^2(l\sin\beta - y_1)^2\right\} = 0\end{aligned} \tag{21}$$

from which one determines the angle β.

Obviously, this method is not the only one which determines the angle β. All the methods lead to a non-linear equation which has to be solved by numerical methods. We preferred to use this method for the simplicity of the partial derivatives of the function described in equation (21).

The partial derivatives of this function are used to determine the derivative of the angle β with respect to the parameter s (the displacement of the valve) and, consequently, the derivative of the same angle with respect to the rotation angle of the crankshaft. These derivatives can be obtained using the theory of the implicit functions.

If the head of the valve is a planar one, then one has to consider in expression (21) that $R_1 \to \infty$, that is, $R_2/R_1 \to 0$.

4. NUMERICAL EXAMPLE

Let us consider as known values the following data: β_0=30°, l=50 mm, R_2=5 mm, R_1=25 mm, s=12 mm. It successively results

$$\begin{aligned}x_1 &= d = l\cos\beta_0 = 43.30127\,\text{mm} \quad h = l\sin\beta_0 + R_2 = 30\,\text{mm} \\ y_1 &= h + s - R_1 = 7\,\text{mm} \quad A_3 = R_1^2 - R_2^2 + l^2 - \left(x_1^2 + y_1^2\right) = 1451\,\text{mm}\end{aligned} \tag{22}$$

The solutions of the equation (21) are

$$\beta_1 = 45.0° \quad \beta_2 = 57.4° \tag{23}$$

Obviously, only the value β_1 will be kept.

The diagrams of variation of the angle β in function of the parameters R_1, R_2 and s are captured in Figures. 2, 3, and 4.

Analyzing these figures one may conclude that the angle β increases when the radius R_1 increases, and it decreases when the radius R_2 increases. These variations are non-linear ones, and the influence of the radius R_1 is greater than that of the radius R_2. The variation of the angle β in function of the valve's displacement s is a quasi-linear one.

5. DETERMINATION OF THE POSSIBLE VALUES

Using the schema presented in Figure 5, one may write

$$C_2A = \sqrt{l^2 + d^2 - 2ld\cos\beta} \tag{24}$$

$$C_1A = h + s - h_1 = l\sin\beta_0 + R_2 - R_1 + s = l\sin\beta \tag{25}$$

$$\frac{l}{\sin\delta} = \frac{C_2A}{\sin\beta} \tag{26}$$

$$\sin\delta = \frac{l\sin\beta}{\sqrt{l^2 + d^2 - 2ld\cos\beta}} \tag{27}$$

$$C_2C_1 = R_1 - R_2 \tag{28}$$

$$\frac{h_1}{\sin\varphi} = \frac{C_2C_1}{\sin\alpha} \tag{29}$$

$$\sin\varphi = \frac{h_1\cos\delta}{R_1 - R_2} \tag{30}$$

$$\gamma = \alpha + \varphi = 90 - \arcsin\left(\frac{l\sin\beta}{\sqrt{l^2 + d^2 - 2ld\cos\beta}}\right) + \arcsin\left(\frac{h_1}{R_1 - R_2}\sqrt{1 - \frac{l^2\sin^2\beta}{l^2 + d^2 - 2ld\cos\beta}}\right) \tag{31}$$

From the bending condition of the valve (due to the eccentricity of the contact point, the valve is acted by an eccentric force during its operation cycle, that is, this force has a maximum value obtained from the theory of the strength of materials), the angle γ is limited to a maximum value

$$\gamma \le \gamma_{\max} \tag{32}$$

and from the formula (31) we get

$$\arcsin\left(\frac{l\sin\beta}{\sqrt{l^2 + d^2 - 2ld\cos\beta}}\right) - \arcsin\left(\frac{h_1}{R_1 - R_2}\sqrt{1 - \frac{l^2\sin^2\beta}{l^2 + d^2 - 2ld\cos\beta}}\right) \ge 90 - \gamma_{\max} \tag{33}$$

relation from which one determines the maximum value $\beta_{\max}$.

In the case of the considered numerical example, taking $\gamma_{\max}$=60°, one obtains the value

$$\beta_{\max} = 55.1^0 \tag{34}$$

6. CONCLUSION

In this paper we performed a geometric study of the contact between the lever and the head of the valve for a spherical contact. We determined the rotation angle of the lever and its maximum values resulted from the bending condition of the valve.

Lucrare prezentată în cadrul Congresului Internațional de Inginerie a Autovehiculelor și Transporturilor - CONAT 2016, 26.10 – 28.10.2016, Brașov, România, și publicată în Proceedings of the Congress (ISSN 2069-0401).

REFERENCES:

[1] Pandrea, Nicolae, Popa, Dinel, Stănescu, Nicolae - Doru: *Classical and Modern Approaches in the Theory of Mechanisms*. John Wiley & Sons, Chichester (2016);

[2] Mihalcea, S, Stănescu, Nicolae - Doru, Popa, Dinel, *Synthesis and kinematic and dynamic analysis of a variable valve lift mechanism with general contact curve*, Proceedings of the International Institution of Mechanical Engineers, Part K, Journal of Multi-body Systems, vol. 229(1), Pages 65–83, 2015, DOI: 10.1177/1464419314546921.

[3] Clenci, A-C, Hara, V, Stănescu, N–D, Bîzîiac, A, Niculescu, R, *Analytical synthesis and computer-aided kinematic analysis of a continuously variable valve lift mechanism*, Proceedings of the International Institution of Mechanical Engineers, Part C, Journal of Mechanical Engineering Science, 2015 (in press).

[4] Stănescu, Nicolae - Doru, Dragomir, Ionuț, Clenci, Adrian, Popa, Dinel, *Synthesis of the Cams Using the Jarvis March*, University of Pitesti, Scientific Bulletin, Automotive Series, 2015.

THERMODYNAMIC PROCESS MODELING IN PRESSURE WAVE SUPERCHARGERS

MODELAREA PROCESELOR TERMODINAMICE ÎN COMPRESOARELE CU UNDE DE PRESIUNE

REZUMAT

Tehnologia undei de presiune s-a dovedit un potențial real în ceea ce privește îmbunătățirea performanței și eficienței sistemelor termodinamice. Principiul său de lucru se bazează pe transferul de energie dintre două fluide care intră în contact direct pentru o perioadă foarte scurtă de timp. Această tehnologie a fost implementată în diverse aplicații inclusiv: turbocompresoare cu unde de presiune în cadrul motoarelor cu combustie internă, camere de combustie cu rotor de unde cu volum constant, mașini frigorifice cu rotor de unde, ultra-micro turbine de gaz, dispozitive de curățare cu schimb de căldură etc.

Această lucrare este o analiză teoretică a evoluției presiunilor de-a lungul canalelor rotorului de undă pentru gazele de eșapament și pentru aerul proaspăt. Mai mult decât atât, o simulare a fenomenului la contactul dintre cele două fluide este furnizată pentru a arăta interacțiunea fluidului cu un nivel ridicat de energie cu fluidul cu un nivel scăzut de energie. Analiza teoretică a fost făcută cu ajutorul software-ului COMSOL Multiphysics. Rezultatele studiului au fost reprezentate grafic. Simularea a fost modelată pentru a reproduce date, cum ar fi presiunile, fluxurile masice și vitezele de obicei măsurate în timp real ale turbocompresoarelor cu unde de presiune ale motorului. Rezultatele au fost obținute la un interval de timp de funcționare diferit cu scopul de a mări presiunea înaltă în colectorul de admise care poate asigura un răspuns mai bun în ceea ce privește creșterea puterii motorului.

Key-words: *Wave rotors, pressure wave supercharging, internal combustion engines, shock waves, rotor channels.*

Drd. ing.
Iuliana COSTIUC
costiuciuliana@unitbv.ro

Prof. dr. ing.
Anghel CHIRU

Universitatea Transilvania din Brașov, Str. Politehnicii nr. 1, 500024 Brașov, România

1. INTRODUCTION

A key priority for the European Union and other nations is preventing the climate change by reducing substantially the greenhouse gas emissions, the main cause of the increase in global temperature [1]. One EU key target for 2020 is cutting 20% in greenhouse gas emissions compared with 1990, as well as 40% cut for 2030 [1]. The long-term consequences of the climate change have led to legislative measures meant to reduce the high levels of pollution, mainly caused by its primary factor: burning fossil fuels.

As the propulsion systems are the main consumers of fossil fuels, it is stated that the road transport sector is responsible for about a fifth of greenhouse gas emissions in Europe [2]. Therefore, the internal combustion engines (ICE) became the primary object for energy conservation and emission reduction in the world [3 in 4]. Under the circumstances, higher energy utilization efficiency and lower emissions are the two major development momentums for IC engine [4].

An optimized thermal management of the ICE and new design of its auxuliary elements can make possible the achievement of the major goals outlined above, by improving the energy utilization efficiency and overall performance, by waste heat recovery, by lowering the fuel consumption, thus lowering the gas emissions.

Since the higher IC engine thermal efficiency appears in the higher load area, boosting pressure becomes one of the effective methods to improve IC engine thermal efficiency [4].

The most important parameters of the power production are: the engines' rotational speed, the engine displacement and the intake manifold pressure [5].

The designers can intervene into modifying the engine displacement or the intake pressure, since the speed in function of the operation needs. The displacement cannot be increased without increasing the friction losses, resulting thus a lowering in the engine's efficiency. Therefore, the most convenient way to increase the power production is to raise the intake manifold pressure, concept generally known as supercharging. It is realized through the use of superchargers or turbochargers. Superchargers and turbochargers are compressors positioned on the admission part of the engine in order to rise the pressure of the incoming air. By using the mechanical supercharging, the improvement to ICE thermal efficiency is very limited because part of ICE effective work is consumed to drive the compressor [4]. Another conventional approach of boosting pressure is exhaust turbocharging, which uses IC engine exhaust gas energy to drive the compressor through exhaust turbocharger. Turbochargers are the most commonly used solutions for car manufacturers to produce useful boost as they have more advantages, e.g., higher thermal efficiency, for the compressor power comes from exhaust gas energy rather than IC engine effective work. However, studies indicate that turbocharging has also some disadvantages [6 in 4] and one of the obvious defects is that it leads to a higher exhaust gas pressure [4].

Many other alternatives succeed to overcome the shortcomings of engine turbocharging; among them, the pressure wave supercharger (PWS) is a promising solution. Pressure wave devices (known as wave rotors) use shockwaves to transfer energy directly between fluids without additional mechanical components, thus having the potential for increased efficiency [7]. In a PWS the interaction between the exhaust high pressure and high temperature gas and the low pressure and low temperature air produce boost. In short terms, the hot gases produce a shock wave that expands through the channels and compresses the fresh air. The rapid response on the engine torque for the entire range of engine speed and the inlet air pulse pressure are reasons for considering the PWS a good option of supercharging the ICE for road vehicles.

The interest on the subject of pressure wave technology present a steady but slow progress. However, since the first real application made by Claude Seippel in 1940, wave rotors have been a research goal for decades [8]. Most of the researches were experimental since the theoretical determinations of the complex phenomena occurring inside a pressure wave device were rather difficult without well-developed computational instruments.

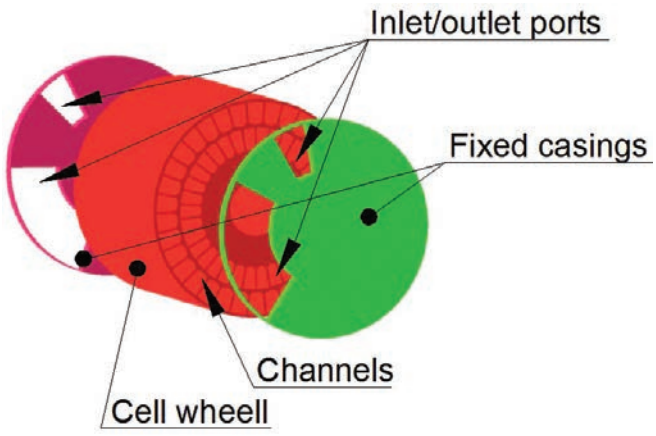

Fig. 1. Main components of a pressure wave supercharger

Recently, new computer software dedicated to accurate simulation of the processes inside the wave rotor devices, together with modern experimental measurements and diagnostic techniques have renewed interest in this technology [8].

2. PW SUPERCHARGING

Principle of Operation: Basically, the PWS is placed in parallel with the ICE within the thermodynamic cycle. PWSs' principle of operation is based on the fact that if two fluids having different pressures are brought into direct contact in long narrow channels, equalization of pressure occurs faster than mixing [9]. The channels are shaped longitudinally into a rotor, called "cell wheel" that rotates between two fixed casings (end plates). The fluids entering the PWS are the high-pressure exhaust gases (HPG) coming from the ICE and the low-pressure air (LPA). As the thermodynamic and pulsatory phenomena occur inside the channels, the resulting fluids leaving the PWS are low pressure gases (LPG) that suffered an extension process into the channels and the compressed air (HPA) leaving the PWS at a higher pressure.

The cell wheel is driven by a separate motor or a belt driven by the crankshaft. The fixed end plates contain passages through which enter the low pressure air and the high pressure gases or exit the high pressure air and the low pressure gases. The ports are connected to the inlet system and the exhaust system, respectively. The exhaust gas inlet port is designed small enough to cause a significant pressure rise in the exhaust manifold [9]. The pressure wave process does not depend on the pressure and flow fluctuations inside the manifold caused by individual cylinder exhaust events; its operation can be explained assuming constant pressure at each set of ports [9].

In Figure 2 is shown the interaction between the components of a four port PWS. The form, dimensions, number and position of ports vary for different applications [10].

Since the end plates that include the ports have fixed positions, the channel ends of the rotor are exposed alternatively to the ports, allowing the fluids flow through the passages.

Thus, the compression and expansion waves are initiated within the PWS channels; the entering gas generates shock waves that evolve along the channel and compress the fresh air.

PWS can be designed for different fluid passage in two configurations, as shown in Figure 2:

a) passing-through flow - when all flows travel in the same direction and

b) reverse flow - when each flow (gas or air) exits on the same side [7] (inlet and outlet ports are placed on the same end plate).

The analysis in this paper is made on a PWS with reverse flow.

The processes inside the narrow channels can be explained using simplified models, presented in the field literature. Basically, the high pressure and high temperature gases exiting from the engine's combustion chamber (HPG) come into contact with the low pressure air (LPA) and a shock wave is formed that starts the compression process. The high pressured air (HPA) leaves PWS towards the inlet manifold while the lowered pressure gases (LPG) are scavenged into the exhaust system.

This paper presents a theoretical analysis of the evolution of the pressures along the channels of a PWS for the exhaust gases and for the fresh air. Furthermore, a simulation of the phenomenon at the contact of the two fluids is provided in order to show the interaction of the high energy fluid with the low energy fluid.

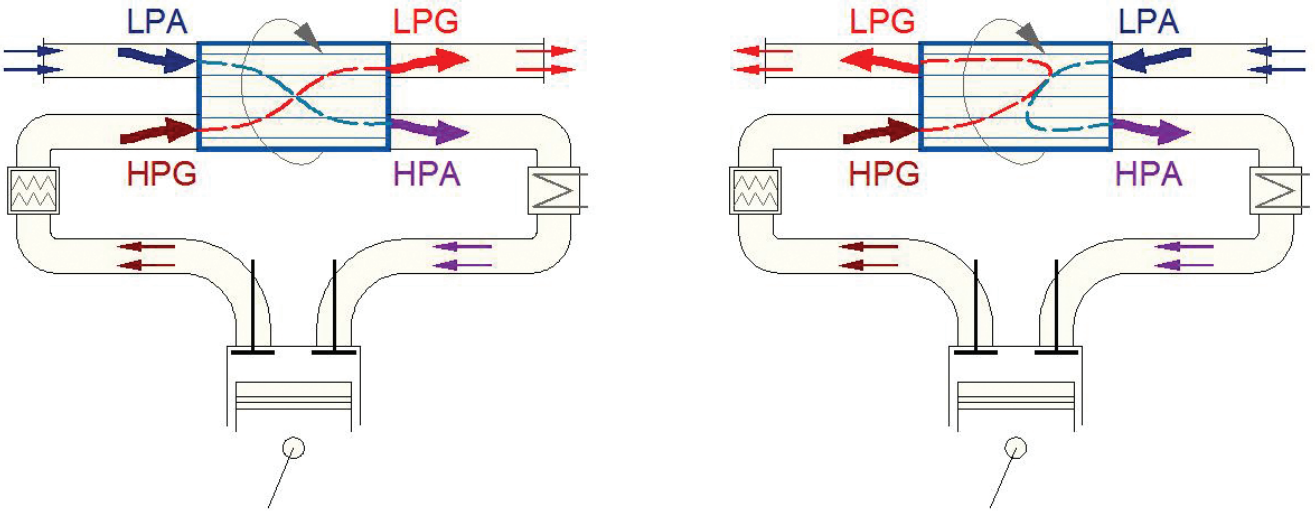

Fig. 2. PWS configurations

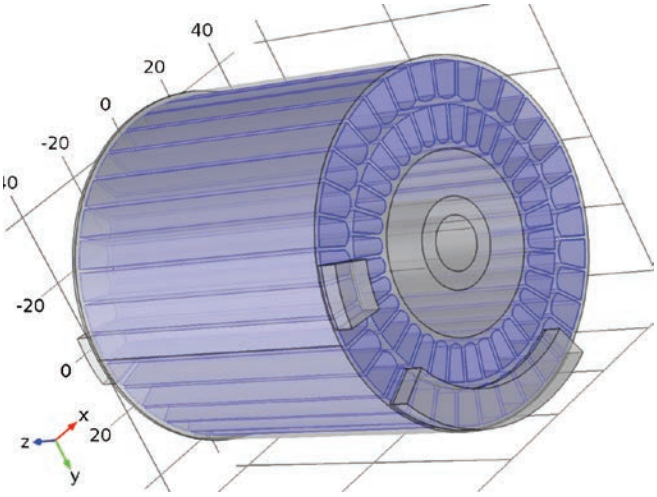

Fig. 3. PWS geometry WS configurations

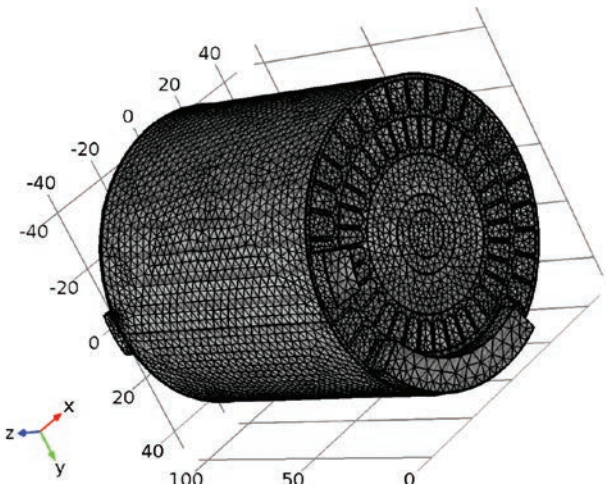

Fig. 4. PWS mesh

Table 1. Entry data for the analytical model

Property	Value
Static gases inlet pressure (p_{gi})	$3.00 \cdot 10^5$ Pa
Static air inlet pressure (p_{ai})	$0.98 \cdot 10^5$ Pa
Inlet gases velocity (u_{gi})	250 m/s
Air specific gas constant (R_{air})	287 J/kg K
Channel length (L)	10^{-2} m
Rotational speed (n_1)	185 s^{-1}

3. NUMERICAL MODEL

In the past years several researchers have investigated compressible flow in PWS channels. Some have been focused on 2D characteristics of the compressible flow [7], other studied the unsteady flow processes in wave rotors [8]. The numerical models used are considered as two-dimensional numerical approaches to save computational time.

In the present work a numerical model was created a three-dimensional numerical model. It was designed to simulate as best as possible conditions in a PWS channels. The 3D-PWS channels are modeled using basic dimensions for CX-93 pressure wave rotor. A gap between exhaust gas plate and air plate with rotor was considered having 1 mm thickness. The rotor was at this step of modeling considered constructed with 2 layers of channels. Air and gases inlets and outlets covers only one layer of channels. The geometry was created in 3D using CAD software, and was imported in Comsol. In Figure 3 is presented only air domain of the geometry. The mesh resulted after some geometry repair operations using internal meshing module is presented in Figure 4 consisting in 283682 tetrahedral elements.

The rotor material used in modeling was considered steel and the fluid used was air. Air was considered as compressible gas. The specific heat, thermal conductivity and the viscosity were considered as temperature dependent. An implicit solver model of Comsol was used, coupling the conservation and momentum equations with the energy equation and the flow was treated as turbulent and time dependent. To simulate the PWS behavior a rotating machinery model was used.

Boundary conditions at inlet and outlet ports were set up as: a pressure inlet on the right side of the inlet gases duct, and a pressure inlet at the left side for fresh air inlet duct. The PWS channels and the ports were initially assumed to be filled with fluid(air) at a reference constant pressure and temperature. A high pressure, high temperature fluid was supplied to the gases inlet duct. To the entire rotating domain containing fluid an axial motion was set up with the rotational speed *n*. The boundary conditions are presented in Table 1.

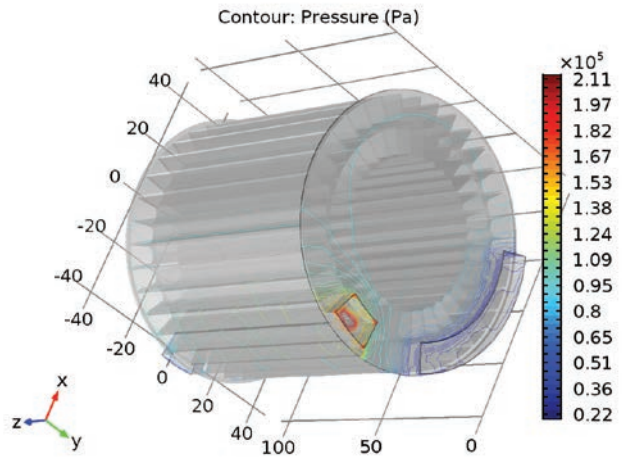

Fig. 5. Pressure contour plot from gas side view

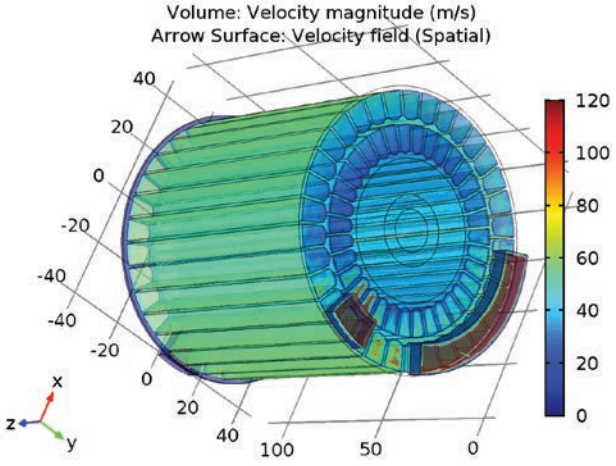

Fig. 6. Velocity field plot from gas side view

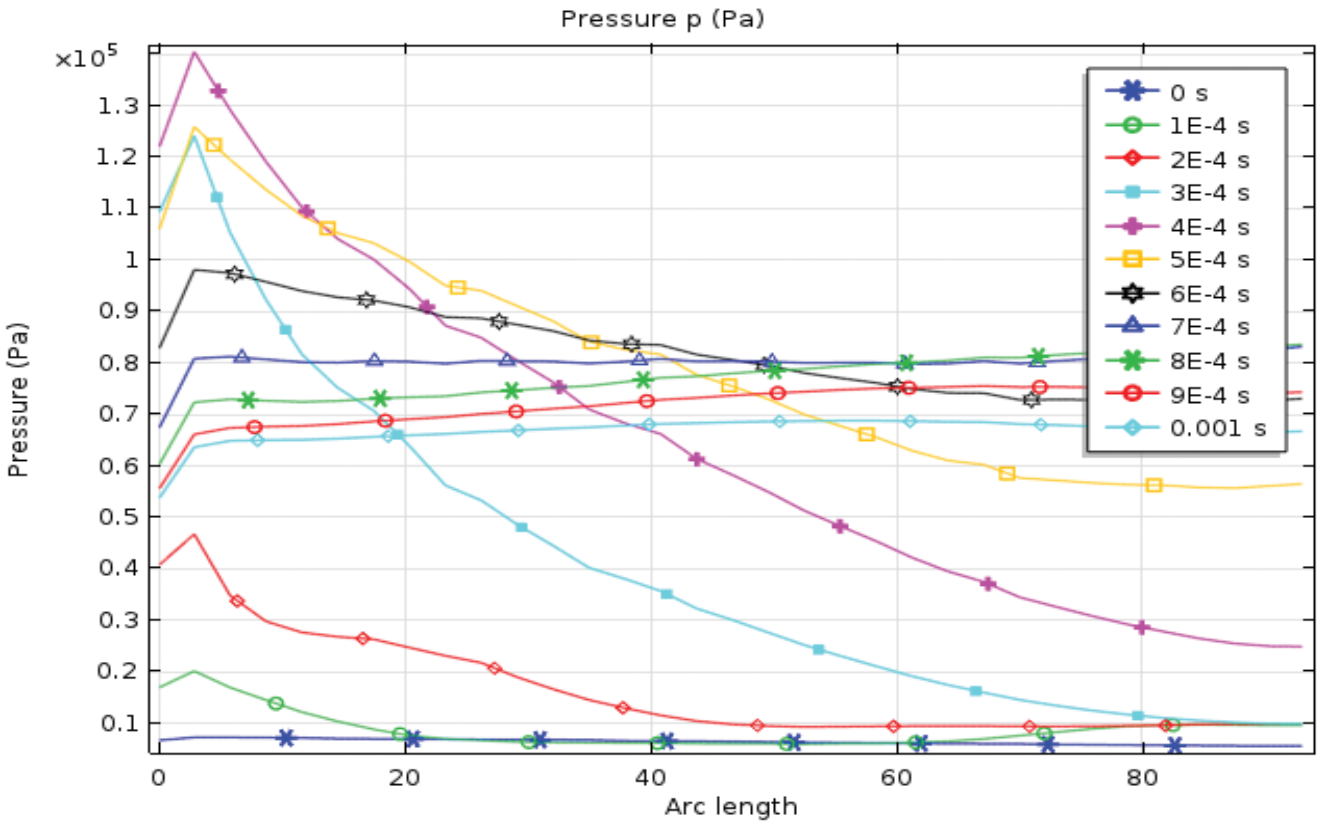

Fig. 7. Pressure plot along a single channel in function of operating time

4. RESULTS

The results obtained with the CFD model described above are presented below. The pressure distribution in PWS channels in contour plot is presented in Figure 5. The velocity field is presented in Figure 6. The pressure distribution in function of time for a single PWS channel in the case of flow that is moving from right to left is presented in Figure 7. In the Figure 5 the pressure plot was obtained for converged stationary regime using boundary conditions for pressure and velocity. The velocity field in Figure 6 was plot in downscale to show the velocities in entire air domain. In the time dependent study the time step in seconds was taken as 0.1 10^{-3} s from 0 to 1 10^{-3} s in order to represent the evolution of the pressure wave along the PWS channel. The pressure evolution in function of time for a single PWS channel (Figure 7) shows that the pressure wave reaches a maximum value of 1.38 10^{5} Pa at 0.4 10^{-3} s.

5. CONCLUSION

The 3D model was developed to investigate the PWS dynamics in order to generate an instrument to improve the engine performance. Using improved 3D CFD numerical methods appears to be a promising solution. The pressure and velocity profile inside the PWS channels were obtained and graphically represented.

Also a time dependent study was performed and the pressure wave profile along PWS channel was presented. All theoretical and numerical results presented were made in order to set-up a 3D numerical model to improve the PWS efficiency. The experimental results from existing literature and the future experimental data will be used for further validation of the presented 3D model. In the next steps research will be extended in stationary and dynamic regimes to reveal the influence of various state, functional and geometrical parameters on the dynamic phenomena of pressures, air velocities, exhaust gases and on the PWS pockets and channels.

Lucrare prezentată în cadrul Congresului Internațional de Inginerie a Autovehiculelor și Transporturilor - CONAT 2016, 26.10 – 28.10.2016, Brașov, România, și publicată în Proceedings of the Congress (ISSN 2069-0401).

REFERENCES:

[1] http://ec.europa.eu/clima/citizens/eu/index_ro.htm - European Comision - Climate Action

[2] http://www.eea.europa.eu/ EEA, 2015b, Monitoring CO2 emissions from new passenger cars and vans in 2014. EEA Technical report No 16/2015, European Environment Agency.

[3] Fu, JQ, Liu, JP, Xu, ZX, Ren, CQ, Deng, BL.: *A combined thermodynamic cycle based on methanol dissociation for IC (internal combustion) engine exhaust heat recovery*. Energy 55:778–86 (2013)

[4] Fu, J, Liu, J., Wang, Y., Deng, B., Yang, Y., Feng, R., Yang, J.: *A comparative study on various turbocharging approaches based on IC engine exhaust gas energy recovery*, Applied Energy 113 (2014) 248–257

[5] Spring, P.: *Modeling and Control of Pressure-Wave Supercharged Engine Systems*, Diss. ETH No. 16490, Swiss Federal Institute of Technology, ETH Zurich (2006)

[6] Liu, JP, Fu, JQ, Ren, CQ, Wang, LJ, Xu, ZX, Deng, BL: *Comparison and analysis of engine exhaust gas energy recovery potential through various bottom cycles*. Appl Therm Eng;50:1219–34 (2013)

[7] Iancu, F., Piechna, J., Müller, N., *Basic design scheme for wave rotors*, Shock Waves (2008) 18:365–378, DOI 10.1007/s00193-008-0165-7, Springer Verlag (2008)

[8] Frackowiak, M., Iancu, F., Potrzebowski, A., Ackbari, P., Müller, N., Piechna, J.: *Numerical Simulation of Unsteady - Flow Processes in Wave Rotors*, Proceedings of IMECE04 2004 ASME International Mechanical Engineering Congress, Anaheim, California USA, November 13–19 (2004)

[9] Heywood, J.: *Internal Combustion Engine Fundamentals*, McGraw-Hill International Editions, I. Title, II. Series (1988).

COMPETIȚIA STUDENȚEASCĂ KART LOW COST LA CEA DE-A 7-A EDIȚIE

KART LOW COST – 7TH EDITION

În 18, 19 mai 2017, Institut Supérieur de l'Automobile et des Transports de Nevers (ISAT), Université de Bourgogne, a găzduit cea de-a șaptea ediție a competiției studențești Kart Low Cost.

Participanții au fost: Université de Bourgogne, ISAT de Nevers (cu un kart termic și unul electric), Universitatea din Pitești (cu două karturi termice și unul electric) - ambele la cea de-a 7-a participare, Universitatea din Craiova (la cea de-a 2-a participare) și Universitatea Politehnica București (la prima participare) - ambele, cu câte 2 karturi termice.

Prima zi a concursului a fost dedicată prezentării și analizei proiectelor tehnice ale echipelor participante. Reamintim că această competiție are scopul de a concepe, proiecta și construi un go-kart cu un buget de 2000 euro pentru propulsia termică, respectiv 3500 euro pentru cea electrică. Dezvoltarea kartului este supusă unor constrângeri tehnice, economice și de timp ce sunt menționate printr-un regulament tehnic precis. Toată această activitate de dezvoltare este completată de testarea karturilor într-o competiție sportivă. Altfel spus, prin intermediul acestei competiții, se încearcă reproducerea la scară redusă a tuturor etapelor de dezvoltare existente în mediul industrial. Prin urmare, obiectivul principal al competiției este dezvoltarea abilităților de gestiune a proiectelor, prin încurajarea muncii în echipă, repartizarea sarcinilor de lucru, respectarea unui buget, noțiuni de sinteză și de compromis ce rezultă din dezvoltarea unui caiet de sarcini.

A doua zi a competiției a fost dedicată probelor sportive prevăzute: sprint, anduranță și slalom. În această etapă se demonstrează faptul că proiectul tehnic dezvoltat de studenți a fost sau nu, unul de succes.

Clasamentul final a fost realizat prin cumularea punctajelor obținute de participanți pe parcursul celor două zile de concurs, astfel că s-au obținut următoarele rezultate:

- Universitatea din Pitești, locul I (kart termic), locul I (kart electric),
- Universitatea Politehnica București, locul II (kart termic),
- Universitatea din Craiova, locul III (kart termic),
- ISAT de Nevers, locul IV (kart termic), locul II (kart electric).

Competiția Kart Low Cost este rezultatul colaborării dintre Université de Bourgogne, ISAT de Nevers, France și Universitatea din Pitești, Departamentul Autovehicule și Transporturi, prima ediție derulându-se în 2011, la Nevers. De atunci, competiția a fost organizată alternant, o dată în Franța, o dată în România.

SIAR a susținut competiția încă de la lansarea sa și încurajează universitățile membre să se implice.

Așadar, ediția a 8-a a Challenge Kart Low Cost va avea loc în cursul lunii mai a anului 2018, undeva în România – evident. Rămâne ca acest detaliu să fie stabilit după ce vom cunoaște echipele participante din România.

Mai multe detalii la:
Cătălin ZAHARIA (catalin.zaharia@upit.ro),
Adrian CLENCI (adrian.clenci@upit.ro)

REGISTRUL AUTO ROMÂN

www.rarom.ro

PROGRAMĂRI
021/9672

www.autotestmagazin.ro
www.facebook.com/RegistrulAuto
www.facebook.com/autotestmagazin